Curved quantum waveguides in uniform magnetic fields

O. Olendski*
Atomic and Molecular Engineering Laboratory, Belarusian State University, Skarina Avenue 4, Minsk 220050, Belarus

L. Mikhailovska
Department of Higher Mathematics, Military Academy, Minsk 220056, Belarus

(Received 23 August 2005; revised manuscript received 3 October 2005; published 12 December 2005)

A theoretical study of a planar electronic waveguide with a uniformly curved section in the perpendicular homogeneous magnetic field **B** is presented within the envelope function approximation. Utilizing analytical solutions in each part of the waveguide, exact expressions are derived for the scattering and reflection matrices and for the transcendental equation defining bound-state energies. It is shown that in the magnetic field a propagation threshold in the continuously curved channel is always smaller than its counterpart for the straight arm which means that bound states in the uniform magnetic field always exist. Their energies do not depend on the direction of the field, and at high magnetic intensities they approach the lowest Landau level. For the transport in the fundamental mode an interaction of a quasibound level split off from the higher-lying threshold as a result of the bend, with its degenerate continuum counterpart, causes a dip in the transmission. In the magnetic field, contrary to the field-free case, conductance in the minimum G_{min}, generally, ceases to be zero. It is shown that growing magnetic fields cause G_{min} to saturate to $2e^2/h$ which means that a quasibound level formed as a result of the bend is completely dissolved by the increasing **B**; however, this transformation is very different for the different bend angles and radii. In particular, quasibound states of the fundamental propagation mode survive stronger fields for the smaller bend angles which is explained by the larger total magnetic flux through the curved section where these levels are formed. Since a magnetic length $l_B=(\hbar/eB)^{1/2}$ is inversely proportional to the square root of B, states for the waveguide with a smaller radius also survive stronger fields, and their asymptotic approach to the dissolution possesses nonmonotonic G_{min} dependence on the magnetic field with minimum conductance again reaching zero for some special values of B. Vortex structure of the currents flowing in the waveguide near the resonance is strongly affected by the field. In particular, small magnetic intensities change zero-field vortices in the straight arms into the magnetic antivortices which correspond to the interacting with each other surface currents flowing along opposite walls of the channel. Increasing the magnetic field suppresses the formation of the vortices pushing currents to the outer (inner) walls in the straight (bent) section. For fields larger than the saturation magnetic intensity, the only consequence of the bend is a strong surface current near the convex wall of the bend, and the electronic flow along the junctions between straight and curved parts.

DOI: 10.1103/PhysRevB.72.235314 PACS number(s): 73.63.−b, 75.75.+a, 73.21.−b

I. INTRODUCTION

The discovery of the quantum Hall effect[1] stimulated intensive theoretical and experimental research on magnetic field influence on low dimensional nanostructures (see Refs. 2–6, and references therein). In particular, the resistances of a quantum channel with a finite barrier inside were calculated in the limit of very strong magnetic fields.[7] Oscillations which are periodic in the field, in the low-temperature magnetoresistance of a point contact in the two-dimensional electron gas were observed experimentally and explained theoretically as a tunneling between edge states across the point contact.[8] Conductivity of the many-terminal junctions of quantum wires was theoretically investigated,[9–11] and a rich structure of the Hall resistance deviating considerably from the wide-wire result was shown. Computational study of several different kinds of four-terminal junctions showed that the Hall and bend resistances are extremely sensitive to the geometry of the junction and that the classical and quantum mechanical results are qualitatively similar but quantitatively very different.[12] Spectroscopy of the energy levels and associated currents of infinitely deep[13,14] and finite[15] quantum wells in crossed magnetic and electric fields was calculated, and a crucial role of the energy spectrum anticrossings in the jumps of the equilibrium Hall currents was described. Theoretical analysis revealed that the magnetic field applied to the straight quantum wire with symmetrically embedded quantum dots leads to the Fano resonances[16] on the conductance Fermi energy dependence.[17–21] It was predicted that asymmetric Fano resonances occur also in the electronic conductance across a shallow quantum well in a high tilted magnetic field.[22]

Standard Hall bar geometry consists of the intersections of planar circuits of narrow wires[5,11,23,24] and, in fact, presents a quantum waveguide with a set of the bends. Therefore, a correct description of the bent quantum wire in the magnetic fields is a significant theoretical and experimental problem. Even though the wave dynamics in the bent waveguide has been a subject of intensive research for more than a century in acoustics[25] and electrodynamics and optics,[26–29] only relatively recently has it been proved theoretically that a field-free bent quantum waveguide with Dirichlet boundary conditions supports localized modes with energies below the fundamental threshold of the straight waveguide.[30–33] Extra

space in the bend presents a shelter where the electrons can dwell with momentum smaller than the cutoff momentum of the lowest subband. Theoretical predictions of the existence of such bound states were confirmed experimentally.[34] Bending of the waveguide leads also to steep dips on the conductance versus Fermi energy dependence.[35–39] These narrow antiresonances lying closely below each propagation threshold are explained by the interference of the discrete level split off by the bend from the higher subband, and continuum states of the lower mode. Recent surveys of the research on the field-free bent quantum waveguides may be found in reviews.[40,41] Miscellaneous aspects of different configurations of bent guiding structures have been under the scrutinized attention of the researchers from different branches of physics, and this interest is not fading.[42–81]

Effects of applied magnetic fields on the properties of the bent waveguides were considered by a number of groups. Influence of the uniform magnetic field on a two-probe conductance of a curved quantum wire was theoretically analyzed in Refs. 82–84. Calculations proved that the hollow bent and twisted quantum tubes of constant cross sections threaded by an Aharonov-Bohm flux[85] also support bound states.[86,87] General gauge suitable for the investigation of the two-dimensional bent quantum wires in a perpendicular magnetic field was discussed.[88] Transmission properties of *L*, *T*, and *X* structures subjected to the superposition of the uniform magnetic field and high frequency radiation were calculated,[89] and the resonant anomalies of the Hall resistance were found in a weak magnetic field. Electronic transport in the infinitely thin curved quantum wire subjected to the Aharonov-Bohm-like magnetic field perpendicular to the waveguide plane, was considered.[90] Theoretical analysis of the bound states of *L*- and *T*-shaped quantum wires in inhomogeneous magnetic fields revealed that the bound-state energy depends quadratically (linearly) on the magnetic field in the weak (strong) fields.[91] Transmission properties of the same structure were also calculated.[92] Electron localization in the bent waveguide with parabolic transverse confinement in perpendicular uniform magnetic fields was analyzed by means of the perturbation theory with respect to the bending angle.[93] Application of the Hardy-type inequality for the magnetic Dirichlet form in the waveguide proved that bounded differentiable fields with compact support or an Aharonov-Bohm field can wipe out bound states of the curved quantum channel.[94] Experimentally, quenching of the quantum Hall effect was observed in a one-dimensional conductor in small magnetic fields.[23] Miscellaneously shaped cross geometries of high-mobility GaAs-$Al_xGa_{1-x}As$ heterostructures were fabricated, and their measured magnetotransport properties were explained by the simple semiclassical picture describing the geometrical scattering of the electrons entering the cross section.[95] Applicability of such an explanation was theoretically confirmed by the exact quantum mechanical consideration.[96] Magnetoluminescence experiments with *V*-shaped (Ref. 97) and *T*-shaped (Ref. 98) quantum wires were corroborated by the direct solution of the corresponding Schrödinger equation. Quantum magnetotransport experiments in periodic *V*-grooved $GaAs/AlGa_xAs_{1-x}$ heterostructures were reported recently.[99] External magnetic field applied parallel to one of the arms of *L*-shaped strained n-$InGa_xAs_{1-x}$ channels was used to investigate experimentally polarization and rotation of electron spins, and it was proved that current-induced spin polarization can be achieved by means of the electric field only.[100]

In the present paper, we return to the theoretical study of the planar quantum waveguide with uniformly curved sections in the perpendicular homogeneous magnetic fields. Within effective-mass approximation and noninteracting electron picture exact analytical solutions are presented in each region and matched at the boundaries between them. Comparative analysis between this and other known approaches is provided. In particular, knowledge of the analytical solutions allows one to derive limiting cases of vanishing and strong magnetic fields. Another advantage of this method lies in the fact that, by matching wave functions at the junctions between curved sections and straight arms, one can either derive formal exact expressions for the scattering and reflection matrices or arrive at the transcendental equation with its solutions defining energies of the bound states of the system. Armed with this knowledge, we provide a comprehensive analysis of both the bound levels as well as scattering states in the wide range of the bend parameters and the fields. For example, an equation is derived for the correct determination of the propagation thresholds in the continuously curved wire. It is shown that bound states of the considered structure always exist, approaching for high magnetic intensities the lowest Landau level. The direction of the field does not influence their properties. Their peculiar feature is the fact that after some field strength that is dependent on bend parameters, the localized level wave function is described by the states with negative angular wave vectors only. For the propagation in the fundamental mode it is shown that a minimum of the conductance at the resonance generally ceases to be zero in nonzero fields. For quite strong magnetic intensities dependent on the bend parameters, the resonance is completely washed out. Quasibound states for the waveguide with smaller bend angles survive stronger fields since a total magnetic flux through such bends is smaller. Also, there is a drastic difference between the conductance behavior for large and small radii with quasibound levels for the former case disappearing at smaller fields. Properties of the conductance in the magnetic field are explained by considering currents flowing in the waveguide. Similarities and differences between current vortices near the resonance for zero and nonzero fields are discussed. It is shown that the increasing field pushes currents in the straight (bent) arm closer to the outer (inner) surface and suppresses the formation of the vortices leading for small magnetic intensities to the antivortices in the straight arms, and when the resonance completely disappears, there is a perfect laminar flow both in the straight arms as well as in the curved section.

The paper is organized as follows. In Sec. II our model is presented and a necessary formulation of our method is given. Several advantages of this approach are also discussed. Section III is devoted to the presentation and detailed physical interpretation of the calculated results. A summary of the results is provided in Sec. IV. In the Appendix we write the explicit form of the scattering and reflection matrices and the transcendental equation for bound state energies.

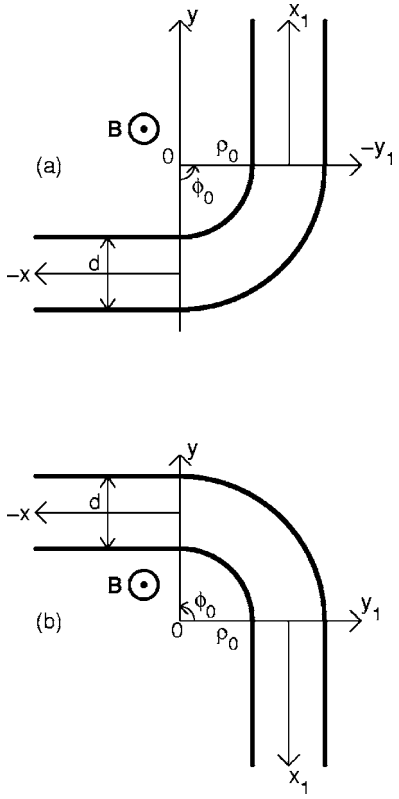

FIG. 1. Up- (a) and down-turn (b) curved quantum waveguide in uniform magnetic field **B** pointing in the positive z direction. Waveguide width is d, bend angle and inner radius are ϕ_0 and ρ_0, respectively. Origin of the polar coordinate system (ρ,ϕ) coincides with the center of the bend. For the case (a) polar axis is a vertical junction of the straight and curved parts, while for the case (b) it is the junction with the right straight channel. Curved arrows show direction in which the azimuthal angle ϕ grows. Local Cartesian coordinate systems (x,y) and (x_1,y_1) for the straight arms are also shown. Their origins coincide with the middle of the corresponding junction with the bent part.

II. MODEL AND FORMULATION

The structure we consider is shown schematically in Fig. 1. The quantum waveguide of width d with hard-wall boundaries is subjected to a homogeneous magnetic field **B** applied in the z direction. The waveguide contains a uniformly curved section with the inner radius ρ_0 and angle ϕ_0. Since, in general, for nonzero magnetic field there is a difference between up- and down-turn bends,[83] both these situations are shown in the figure and are discussed later in the text. We assume noninteracting electron picture within effective-mass approximation.[101] Electron spin splitting is neglected. Then, in the time-independent single-particle Schrödinger equation describing the electron wave function $\Psi(\mathbf{r})$

$$\left[\frac{1}{2m^*}(-i\hbar\,\boldsymbol{\nabla}+e\mathbf{A})^2+V(\mathbf{r})\right]\Psi(\mathbf{r})=E\Psi(\mathbf{r}), \tag{1}$$

where e is an absolute value of the electronic charge, m^* is an effective electron mass, $c\equiv 1$, the electrostatic potential $V(\mathbf{r})$ is zero inside the waveguide and infinity otherwise. In addition, a magnetic field enters Eq. (1) via the vector potential **A**, $\mathbf{B}=\boldsymbol{\nabla}\times\mathbf{A}$.

It is convenient at this point to introduce dimensionless variables; namely, we will measure all distances in units of the waveguide width d; all energies, in units of ground-state energy $\pi^2\hbar^2/(2m^*d^2)$ of the infinite quantum well of width d; all momenta, in units of $1/d$; magnetic fields, in units of $\hbar/(ed^2)$; time, in units of $2m^*d^2/(\pi^2\hbar)$; conductance, in units of $2e^2/h$; magnetic flux, in units of h/e; and two-dimensional current density, in units of $e\hbar/(m^*d^3)$.

In the straight waveguide to the left of the bend, Eq. (1) may be solved in the separable form in the Cartesian coordinate system (x,y) shown in Fig. 1 and with the Landau gauge for the vector potential $\mathbf{A}=(-yB,0)$:

$$\Psi(x,y)=\exp(ipx)\chi_p(y), \tag{2}$$

where function $\chi_p(y)$ satisfies the equation

$$\left(\frac{d^2}{dy^2}+[\pi^2E-(By-p)^2]\right)\chi_p(y)=0 \tag{3}$$

with the boundary conditions $\chi_p\left(\pm\frac{1}{2}\right)=0$.

Since a direct numerical integration of Eq. (3) was performed in Refs. 11 and 84, we adopt here another method of its solution; namely, we have found it more convenient to present a solution in the analytical form:

$$\begin{aligned}\chi_{p_n}(y)=\gamma_{p_n}\Bigg[&U\left(\frac{\pi^2}{2}\frac{E}{B},-i(2B)^{1/2}\left(\frac{1}{2}-\frac{p_n}{B}\right)\right)\\&\times U\left(\frac{\pi^2}{2}\frac{E}{B},i(2B)^{1/2}\left(y-\frac{p_n}{B}\right)\right)\\&-U\left(\frac{\pi^2}{2}\frac{E}{B},i(2B)^{1/2}\left(\frac{1}{2}-\frac{p_n}{B}\right)\right)\\&\times U\left(\frac{\pi^2}{2}\frac{E}{B},-i(2B)^{1/2}\left(y-\frac{p_n}{B}\right)\right)\Bigg].\end{aligned} \tag{4}$$

Function $U(a,\xi)$ in Eq. (4) is a Weber parabolic cylinder function,[102,103] and the unknown coefficient γ_{p_n} is determined from the normalization condition which we choose in the form[11,84]

$$\int_{-12}^{12}(p_n+p_{n'}-2By)\chi_{p_n}(y)\chi_{p_{n'}}(y)dy=\delta_{nn'}, \tag{5}$$

where $\delta_{nn'}$ is a Kronnecker symbol.

Allowed values of the coefficients p_n are to be found from the boundary conditions. A form of the solution, Eq. (4), automatically zeroes the wave function on one of the walls. Applying the same requirement to the second side of the strip, one arrives at the transcendental equation for the determination of the allowed values of p:

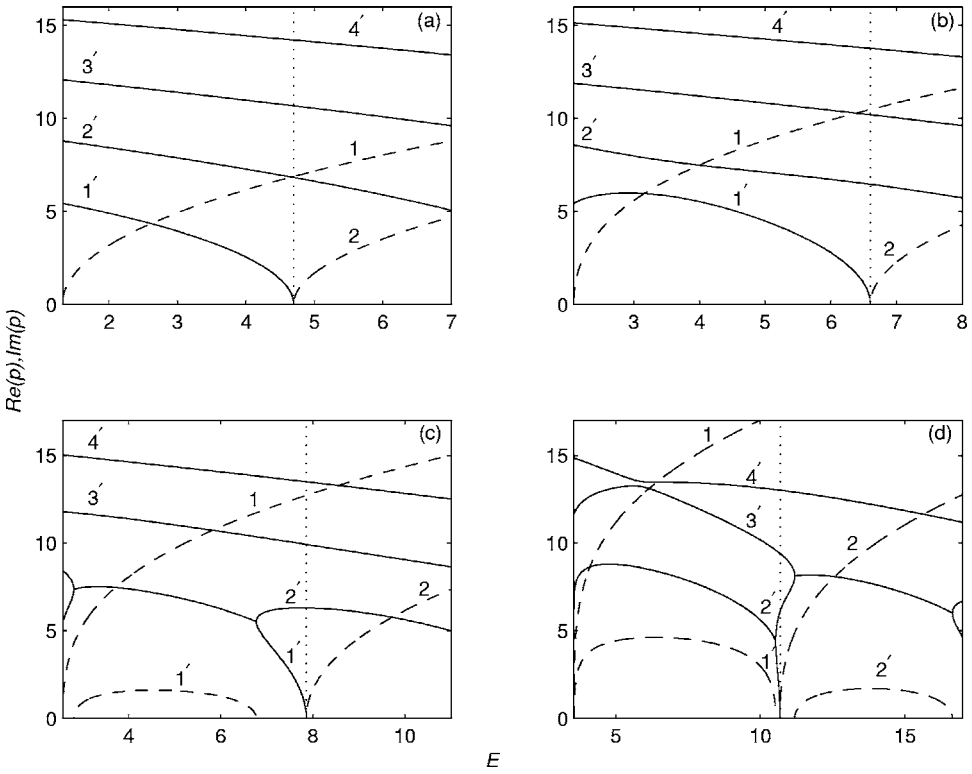

FIG. 2. Momenta p of the straight channel in the magnetic field as a function of the Fermi energy E for several values of B: (a) $B=10$, (b) $B=20$, (c) $B=25$, and (d) $B=35$. Dashed lines are for the real part of the momentum, and the solid ones—for the imaginary constituents. Numbers near the propagating states denote the corresponding subbands, while primed numbers are used for the evanescent or oscillatory damped levels. Dotted vertical lines show first excited subband thresholds for the corresponding magnetic field B. Since, for the high fields, the interval near the fundamental threshold where two levels with lowest imaginary Im(p) are split off, is too small, it is not resolved in (d). Abscissas have different scale for each of the figures.

$$U\left[\frac{\pi^2}{2}\frac{E}{B},-i(2B)^{1/2}\left(\frac{1}{2}-\frac{p_n}{B}\right)\right]U\left[\frac{\pi^2}{2}\frac{E}{B},-i(2B)^{1/2}\left(\frac{1}{2}+\frac{p_n}{B}\right)\right]$$
$$-U\left[\frac{\pi^2}{2}\frac{E}{B},i(2B)^{1/2}\left(\frac{1}{2}-\frac{p_n}{B}\right)\right]$$
$$\times U\left[\frac{\pi^2}{2}\frac{E}{B},i(2B)^{1/2}\left(\frac{1}{2}+\frac{p_n}{B}\right)\right]=0. \quad (6)$$

Note that the left-hand side of Eq. (6) is considered as a function of momentum p_n for fixed values of energy E and magnetic field B. From the properties of the Weber functions[102] it directly follows that Eq. (6) has a countably infinite set of solutions p_n, $n=1,2,\ldots$, with only a finite number of real and infinitely many purely imaginary p_n. The real values of p_n are naturally associated with the propagating waves, while purely imaginary values of the momentum correspond to the attenuated or evanescent modes. For some values of E and B, Eq. (6) can also have complex solutions that correspond to the oscillatory damped states. It was pointed out earlier that such states exist[11,84] and their dependence on the magnetic field was calculated;[11,84,104] below we give their detailed analysis as functions of the Fermi energy for the wide range of the induction B. Note also that this equation is invariant under the transformation $p\to -p$, and Eq. (3) remains the same after the simultaneous change $p\to -p$, $y\to -y$. Some other properties of the functions $\chi_{p_n}(y)$ and coefficients p_n are given in Ref. 11.

Another advantage of the analytical solution in the form of Eq. (4) is the fact that Eq. (6) can be used for finding band edge energies as functions of the magnetic field. Namely, at the band edge $p=0$, and Eq. (6) transforms to

$$U^2\left[\frac{\pi^2}{2}\frac{E}{B},i\left(\frac{B}{2}\right)^{1/2}\right]-U^2\left[\frac{\pi^2}{2}\frac{E}{B},-i\left(\frac{B}{2}\right)^{1/2}\right]=0. \quad (7)$$

This equation implicitly defines band edge energies as a function of B. Equation (7) allows us to analytically derive limiting cases of weak and strong magnetic fields. In particular, by using properties of the Weber functions,[102] one can show that for the vanishing fields the band edge energies tend to $E=n^2$, as would be expected. Along the same lines it can be derived that for large B these energies approach asymptotically from above the equidistant Landau spectrum[105]

$$E=(2n-1)B/\pi^2, \quad (8)$$

a result known from earlier numerical investigation.[11]

Figure 2 shows momenta p_n calculated from Eq. (6) as functions of energy E for several values of the magnetic field B. It is seen that from the lowest subband threshold the magnitude of p for the fundamental propagating mode monotonically increases with energy. For small and moderate magnetic fields absolute values of the imaginary momenta decrease with energy growing, as it is seen from Fig. 2(a). This means higher spatial extent of the corresponding localized state. At the first excited threshold lowest $|p|$ turns to zero, and the second propagating channel with real momentum emerges, as expected. We note that for the ranges of the magnetic fields from Fig. 2(a) the localized levels do not interact with each other. However, the situation changes with further increase of B. One of the initial stages of the interaction of the bound states is shown in Fig. 2(b); namely, lowest $|p|$ does not decrease, as it was the case for the weaker fields, but gets bigger, approaching the nearest higher momentum. For the field from Fig. 2(b) this interaction is still too small.

But on the increase of B two lowest imaginary momenta rapidly are drawn closer, and at $B \simeq 21.631$ these levels touch each other. Their interaction at higher fields leads to the range of energies where their $\mathrm{Im}(p)$ are equal, as it is seen in Figs. 2(c) and 2(d). At the same time, at the energy when the imaginary parts coalesce, real constituents of the momentum cease to be zero, acquiring for each of the states an equal magnitude with the opposite signs. The positive real part of the momentum p is shown in the figure. With energy growing, its magnitude grows also, reaches maximum, starts to decrease, and when it approaches zero again, imaginary parts split off. Thus, we have again two true localized levels. Physically, equal magnitude of the real part of the complex value of the momentum means that the exponentially modulated wave propagates in both directions of the straight waveguide with the same frequency and fading. Energy intervals where exponentially damped waves exist, get broader with the magnetic field growing. In fact, as Fig. 2(d) shows, for large enough intensities B such levels occupy almost the whole fundamental subband splitting only in the very neighborhoods of the subband thresholds. It is also seen that the same interaction takes place for the excited subbands too. Another feature Fig. 2(d) shows is the interaction of the bound states with higher magnitudes of $\mathrm{Im}(p)$. Levels $3'$ and $4'$, which did not interact at lower magnetic fields, strongly anticross and almost touch each other at $B=35$. At higher fields their interaction is identical to that described above.

For our problem a total solution to the left of the bend is

$$\Psi(x,y) = \sum_{n=1}^{\infty} [C_n \chi_{p_n}(y) \exp(ip_n x) + D_n \chi_{-p_n}(y) \exp(-ip_n x)], \quad x \leqslant 0. \tag{9}$$

The first sum in Eq. (9) describes the waves incident on the bend, with a second term being a set of reflected (for the real p_n) or localized near the curve (for the purely imaginary p_n) modes. Complex amplitudes C_n and D_n define the relative contribution of the nth subband into the total current.

Solution after the bend reads

$$\Psi(x_1,y_1) = \sum_{n=1}^{\infty} F_n \chi_{p_n}(y_1) \exp(ip_n x_1), \quad x_1 \geqslant 0. \tag{10}$$

Again, terms in Eq. (10) with real p_n describe the waves propagating away from the curved scatterer, while the terms with purely imaginary momenta are the states trapped by the bend. This equation was derived in the rectangular coordinate system (x_1,y_1) with the vector potential of the following form: $\mathbf{A}=(-By_1,0)$. Similar to the field-free situation,[39,62] for a particular case of C_n being a Kronecker symbol, $C_n=\delta_{nm}$, $m=1,2,\ldots$; due to the conservation law the following relation holds for the energies E such that $E>E_m^{TH}$, with E_m^{TH} being mth solution of Eq. (7):

$$\sum_{n=1}^{\infty} \frac{p_n}{p_m} (|D_n|^2 + |F_n|^2)\, \theta(E - E_n^{TH}) = 1. \tag{11}$$

$\theta(x)$ in Eq. (11) is a step function, and terms $p_n/p_m|F_n|^2$ and $p_n/p_m|D_n|^2$ are, respectively, current transmission and reflection probabilities between subbands m and n.

In the curved section, for the up-turn bend, in the polar system of coordinates (ρ,ϕ) with its origin at the center of the bend and the polar axis coinciding with the vertical junction between the straight and curved parts, the symmetric gauge for the vector potential

$$\mathbf{A} = \left(0, \tfrac{1}{2}B\rho\right), \tag{12}$$

radial and angular variables are separated:

$$\Psi(\rho,\phi) = \sum_{n=1}^{\infty} Q_n R_{\nu_n}(\rho) \exp(i\nu_n \phi), \tag{13}$$

and the radial wave function satisfies the equation

$$\left(\frac{d^2}{d\rho^2} R_{\nu_n}(\rho) + \frac{1}{\rho}\frac{d}{d\rho} R_{\nu_n}(\rho) + \pi^2 E R_{\nu_n}(\rho)\right) - \left(\frac{\nu_n}{\rho} + \frac{1}{2}B\rho\right)^2 R_{\nu_n}(\rho) = 0 \tag{14}$$

with boundary conditions: $R_{\nu_n}(\rho_0)=R_{\nu_n}(\rho_0+1)=0$. Numerical solutions of Eq. (14) were developed in Refs. 82–84 and 106. Instead, here we represent it in the following analytical form:

$$\begin{aligned} R_{\nu_n}(\rho) = \gamma_{\nu_n} \exp\left(-\frac{1}{4}B\rho^2\right)\left(\frac{1}{2}B\rho^2\right)^{\nu_n/2} \times \Bigg[& M\left(\frac{1}{2} + \nu_n - \frac{\pi^2}{2}\frac{E}{B}, \nu_n + 1, \frac{1}{2}B\rho_0^2\right) \\ & \times U\left(\frac{1}{2} + \nu_n - \frac{\pi^2}{2}\frac{E}{B}, \nu_n + 1, \frac{1}{2}B\rho^2\right) \\ & - U\left(\frac{1}{2} + \nu_n - \frac{\pi^2}{2}\frac{E}{B}, \nu_n + 1, \frac{1}{2}B\rho_0^2\right) \\ & \times M\left(\frac{1}{2} + \nu_n - \frac{\pi^2}{2}\frac{E}{B}, \nu_n + 1, \frac{1}{2}B\rho^2\right)\Bigg]. \end{aligned} \tag{15}$$

Here, $M(a,b,x)$ and $U(a,b,x)$ are Kummer confluent hypergeometric functions,[103,107] and γ_{ν_n} is determined from the normalization condition of the form[82–84]

$$\int_{\rho_0}^{\rho_0+1} \left(\frac{\nu_n + \nu_{n'}}{\rho} + B\rho\right) R_{\nu_n}(\rho) R_{\nu_{n'}}(\rho) d\rho = \delta_{nn'}. \tag{16}$$

In order to distinguish the Weber function $U(a,x)$ from the confluent hypergeometric function $U(a,b,x)$, we write each of them with all their variables.

Contrary to the systems with circular symmetry,[96,108–116] in our case the coefficients ν_n are not real integers. Moreover, as it was mentioned in Refs. 82–84, they, in addition to the real values, take complex ones as well. We will discuss this situation in detail. Another difference lies in the fact that for our configuration one needs to get rid of the solution in Eq. (14) of the absolute value $|\nu_n|$, replacing it by ν_n itself.

The boundary condition $\Psi(\rho_0,\phi)=0$ is automatically satisfied by Eq. (15). Imposing the second condition $\Psi(\rho_0+1,\phi)=0$, one gets the transcendental equation for determining the allowed values of ν_n:

$$M\left(\frac{1}{2}+\nu_n-\frac{\pi^2}{2}\frac{E}{B},\nu_n+1,\frac{1}{2}B\rho_0^2\right)\times U\left(\frac{1}{2}+\nu_n-\frac{\pi^2}{2}\frac{E}{B},\nu_n+1,\frac{1}{2}B(\rho_0+1)^2\right)-U\left(\frac{1}{2}+\nu_n-\frac{\pi^2}{2}\frac{E}{B},\nu_n+1,\frac{1}{2}B\rho_0^2\right)\times M\left(\frac{1}{2}+\nu_n-\frac{\pi^2}{2}\frac{E}{B},\nu_n+1,\frac{1}{2}B(\rho_0+1)^2\right)=0. \quad (17)$$

It determines the values of ν for the fixed energies E, fields B, and radius ρ_0.

Putting in Eq. (17) the value of ν_n equal to zero, one can determine the energies of vanishing angular wave vector in the continuously curved waveguide in the uniform magnetic field B:

$$M\left(\frac{1}{2}-\frac{\pi^2}{2}\frac{E}{B},1,\frac{1}{2}B\rho_0^2\right)U\left(\frac{1}{2}-\frac{\pi^2}{2}\frac{E}{B},1,\frac{1}{2}B(\rho_0+1)^2\right)-U\left(\frac{1}{2}-\frac{\pi^2}{2}\frac{E}{B},1,\frac{1}{2}B\rho_0^2\right)M\left(\frac{1}{2}-\frac{\pi^2}{2}\frac{E}{B},1,\frac{1}{2}B(\rho_0+1)^2\right)=0. \quad (18)$$

Equations (17) and (18) deserve some attention. First, we note that the first of them always has solutions for $\nu_n=(\pi^2/2)(E/B)-n+\frac{1}{2}$, and the second one—for the Landau levels, Eq. (8), and the confluent hypergeometric functions in these two equations degenerate into the Laguerre polynomials.[103,107] Such solutions, which are independent of ρ_0 solutions correspond to the usual cyclotron motion without any confining potential. Even though they are mathematically correct, they are spurious from physical points of view and should be neglected for our situation, since for them radial wave functions, Eq. (15), identically turn to zero. Second, it directly follows from the properties of the confluent hypergeometric functions[103,107] that Eqs. (17) and (18) for the vanishing magnetic fields transform into the corresponding equations for the zero-field bend[39]:

$$Y_{\nu_n}(\pi E^{1/2}\rho_0)J_{\nu_n}[\pi E^{1/2}(\rho_0+1)]-J_{\nu_n}(\pi E^{1/2}\rho_0)Y_{\nu_n}[\pi E^{1/2}(\rho_0+1)]=0, \quad (19)$$

$$Y_0(x\rho_0)J_0[x(\rho_0+1)]-J_0(x\rho_0)Y_0[x(\rho_0+1)]=0, \quad (20)$$

J_ν, Y_ν are νth order Bessel functions of the first and second kind, respectively.[103] Radial wave function, Eq. (15), in this case is, apart from the normalization constant [that is not important anyway, since normalization in the bend can be done through the coefficients Q_n in Eq. (13)], the radial distribution in the curve without the magnetic field[39]:

$$R_{\nu_n}(\rho)=Y_{\nu_n}(\pi E^{1/2}\rho_0)J_{\nu_n}(\pi E^{1/2}\rho)-J_{\nu_n}(\pi E^{1/2}\rho_0)Y_{\nu_n}(\pi E^{1/2}\rho). \quad (21)$$

An analysis shows that a complete set of solutions to Eq. (17) consists of zero or several real radial wave vectors and a countably infinite number of complex ν_n. Utilizing again the properties of the confluent hypergeometric functions,[103,107] it is readily shown that if the complex ν_n is a solution to Eq. (17), then its complex conjugate ν_n^* also satisfies the eigenvalue equation, and, accordingly, their wave functions have the same real part and equal but opposite values of the imaginary component. In fact, this conclusion is immediately seen from Eq. (14). Since, contrary to the dropped above solutions, these ν_n depend on ρ_0, semiclassically they correspond to the edge currents,[24,117–119] or "skipping orbits," flowing along the curved surfaces and playing an important role in the explanation of the quantum Hall effect.[2,3,5] Sign of the real part of ν_n shows angular direction in which the electron moves after time averaging. In the limit of zero magnetic fields the coefficients ν_n transform into the set of the wave vectors with a finite number of real and infinitely many purely imaginary values with each of them having its counterpart with the opposite sign.[39,82,83,106]

Figure 3 shows angular wave vectors for $\rho_0=0.01$ and $B=5$ as a function of the energy E. Here, complex states are conveniently numbered by the increasing magnitude of the imaginary parts of ν_n. On increase of the energy, absolute values of the imaginary parts decrease and at some points turn to zero. We see that solutions of two equations—Eq. (18) that can be written in the following explicit form: $\nu_n(E)=0$, and of the equation

$$\left.\frac{\partial E}{\partial\,\mathrm{Im}(\nu_n)}\right|_{\partial^2 E/\partial[\mathrm{Im}(\nu_n)]^2\neq 0}=0, \quad (22)$$

which were identical for the field-free case, are not equivalent in the presence of magnetic fields. For example, for the first complex state from Fig. 3, Eq. (22) is satisfied at $E=0.8819$. At this point, two complex wave vectors turn into two negative ones and, accordingly, we have two surface states with nonzero ν_n while in the absence of the field these wave vectors are zero. One of the wave vectors decreases, and the other one rapidly grows and reaches zero at the energy being a solution of Eq. (18), in particular, in the case of Fig. 3 this takes place at energy $E=0.9425$, and at higher energies corresponding to levels that transform into the surface state carrying current in the opposite direction. The wave number of this surface level grows on further increase of energy. Described procedure of transformation of the complex states into two levels with negative ν_n and their subsequent evolution is the same for the states with higher magnitudes of $\mathrm{Im}(\nu_n)$. For example, a second pair of the complex levels transforms into two surface states with negative ν_n at $E=3.7616$. In a sense, such processes in the curved section are a reminiscense of the analogous coalescences and splittings taking place in the straight arms, as it was considered above. Discussed here asymmetry of the dispersion relation of ν_n is due to the fact that the charged particle motion is fixed by the magnetic field, and thus, clockwise and counterclockwise angular directions are not equivalent as they are for $B=0$. The higher the field, the larger the asymmetry and, accordingly, the larger the difference between the solutions

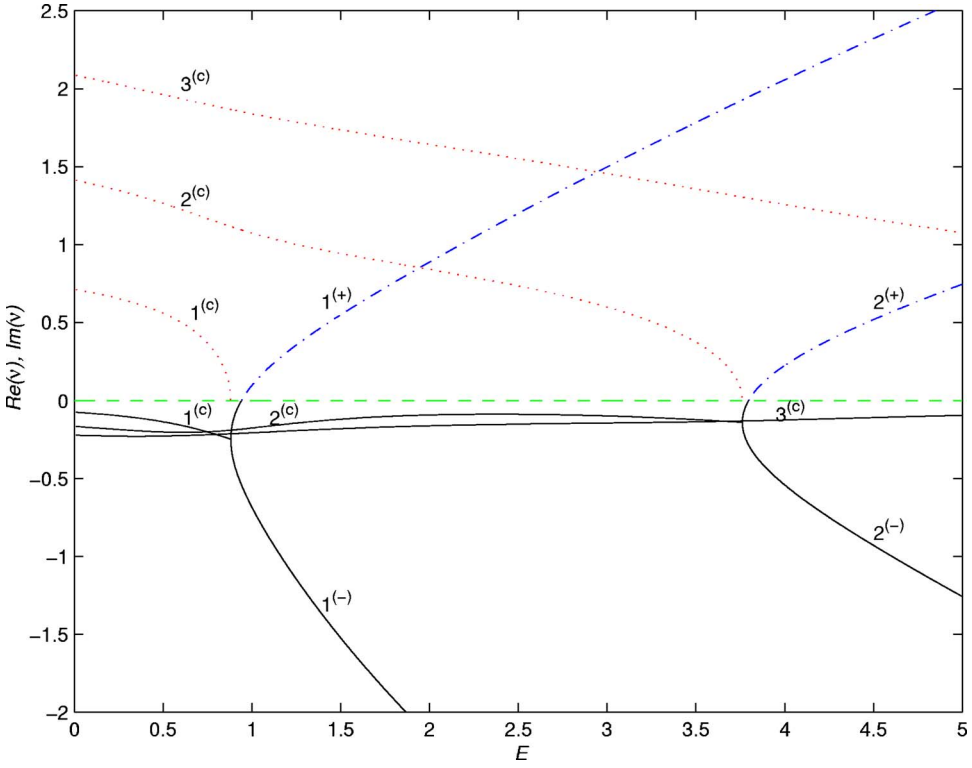

FIG. 3. (Color online) Propagation constants ν_n of the continuously curved waveguide as a function of the energy E for $\rho_0=0.01$ and $B=5$. States with positive (negative) ν_n are plotted by the dash-dotted (solid) lines and denoted by the corresponding superscript near the level numbers. Real parts of the states with complex propagation constants are also shown by the solid lines and denoted by the superscript (c). Imaginary parts of the complex ν_n are plotted by the dotted curves. Dashed line denotes zero value of the angular constant.

of Eqs. (18) and (22). We will exemplify this situation in the next section.

Thus, we have found analytical solutions in each part of the waveguide: Eqs. (9) and (10) describe particle dynamics in the straight arms, and Eq. (13) is the wave function in the bend. Transport properties of the structure in the ballistic regime are completely determined by the scattering matrix $\mathbf{S}(E)$, which relates amplitudes of the incoming and transmitted waves in each subband. In our notation, it is

$$\mathbf{F}=\mathbf{SC}, \tag{23}$$

where amplitudes C_n and F_n from Eqs. (9) and (10) form infinite column vectors $\mathbf{C}$ and $\mathbf{F}$, respectively. Matrix $\mathbf{S}(E)$ is a function of the Fermi energy E. It also depends on the parameters ρ_0, ϕ_0, and B. Knowledge of $\mathbf{S}(E)$ allows one to calculate the two-probe conductance[120]:

$$G(E)=\sum_{nn'}\frac{p_{n'}}{p_n}S^*_{nn'}S_{nn'}, \tag{24}$$

where the scattering matrix element $S_{nn'}$ defines the probability of the electron scattering from channel n to n'. The sum in Eq. (24) runs over all open channels. To find the scattering matrix, one needs to match solutions in the different regions at the junctions between them. However, before doing this, it is necessary to bring the solutions to the form where they are expressed in the same gauge. Recall that solution Eq. (9) was derived in the Landau gauge $\mathbf{A}=(-yB,0)$, the wave function in the second straight arm, Eq. (10), is valid for the Landau gauge $\mathbf{A}=(-y_1B,0)$, and the solution in the bend, Eq. (13), holds true for the symmetric gauge Eq. (12), where vector potentials for the straight arms are written in the corresponding Cartesian coordinates. Basic principles of quantum mechanics[121] require that the change of the vector potential $\mathbf{A}\to\mathbf{A}+\nabla f$ should be accompanied by the corresponding transformation of the wave function: $\Psi(\mathbf{r})\to\Psi(\mathbf{r})\exp(-ief/\hbar)$, with $f(\mathbf{r})$ being an arbitrary function of space. Applying this rule to our situation and choosing as a global gauge the symmetric one, we find that the solution in the left straight arm takes the form

$$\Psi_S(x,y)=\exp\left(-\tfrac{i}{2}Bx\left(y+\rho_0+\tfrac{1}{2}\right)\right)\sum_{n=1}^{\infty}\left[C_n\chi_{p_n}(y)\exp(ip_nx)+D_n\chi_{-p_n}(y)\exp(-ip_nx)\right], \tag{25}$$

where the subscript S shows that we consider solutions in the symmetric gauge. Since a symmetric gauge Eq. (12) does not depend on the azimuthal angle ϕ, additional phase factors in the second straight arm are similar to the one from Eq. (25):

$$\Psi_S(x_1,y_1)=\exp\left[-\tfrac{i}{2}Bx_1\left(y_1+\rho_0+\tfrac{1}{2}\right)\right]\times\sum_{n=1}^{\infty}F_n\chi_{p_n}(y_1)\exp(ip_nx_1). \tag{26}$$

Matching the wave functions at the boundaries, we use, for the up-turn bend [Fig. 1(a)], relations between different systems of coordinates (x,y), (ρ,ϕ), and (x_1,y_1):

$$(x=0,y)\Leftrightarrow\left(-y+\rho_0+\tfrac{1}{2},\phi=0\right), \tag{27a}$$

$$(x_1=0,y_1)\Leftrightarrow\left(-y_1+\rho_0+\tfrac{1}{2},\phi=\phi_0\right), \tag{27b}$$

$$\left.\frac{\partial}{\partial x}\right|_{x=0} \Leftrightarrow \frac{1}{-y+\rho_0+\frac{1}{2}} \left.\frac{\partial}{\partial \phi}\right|_{\phi=0}, \tag{27c}$$

$$\left.\frac{\partial}{\partial x_1}\right|_{x_1=0} \Leftrightarrow \frac{1}{-y_1+\rho_0+\frac{1}{2}} \left.\frac{\partial}{\partial \phi}\right|_{\phi=\phi_0}. \tag{27d}$$

Then, as a result of matching, we have

$$\sum_{n=1}^{\infty} [C_n \chi_{p_n}(y) + D_n \chi_{-p_n}(y)] = \sum_{n=1}^{\infty} Q_n R_{\nu_n}\left(-y+\rho_0+\tfrac{1}{2}\right), \tag{28a}$$

$$\sum_{n=1}^{\infty} \left\{ C_n \left[p_n - \tfrac{1}{2} B\left(y+\rho_0+\tfrac{1}{2}\right)\right] \chi_{p_n}(y) + D_n \left[-p_n - \tfrac{1}{2} B\left(y+\rho_0+\tfrac{1}{2}\right)\right] \chi_{-p_n}(y) \right\} = \frac{1}{-y+\rho_0+\frac{1}{2}} \sum_{n=1}^{\infty} \nu_n Q_n R_{\nu_n}\left(-y+\rho_0+\tfrac{1}{2}\right), \tag{28b}$$

$$\sum_{n=1}^{\infty} Q_n R_{\nu_n}\left(-y_1+\rho_0+\tfrac{1}{2}\right) \exp(i\nu_n \phi_0) = \sum_{n=1}^{\infty} F_n \chi_{p_n}(y_1), \tag{28c}$$

$$\sum_{n=1}^{\infty} \frac{\nu_n}{-y_1+\rho_0+\frac{1}{2}} Q_n R_{\nu_n}\left(-y_1+\rho_0+\tfrac{1}{2}\right) \exp(i\nu_n \phi_0) = \sum_{n=1}^{\infty} F_n \chi_{p_n}(y_1) \left[p_n - \tfrac{1}{2} B\left(y_1+\rho_0+\tfrac{1}{2}\right)\right]. \tag{28d}$$

System of Eqs. (28) allows one to express coefficients F_n through C_n, i.e., according to Eq. (23), to define the scattering matrix $\mathbf{S}(E)$. Its explicit form is given in the Appendix. We also write there the expression for the reflection matrix $\mathbf{R}(E)$ linking amplitudes of incoming and reflected waves in different subbands,

$$\mathbf{D} = \mathbf{R}\mathbf{C}. \tag{29}$$

So far, we have considered the up-turn bend and the magnetic field **B** directed in the positive z direction [Fig. 1(a)]. From the symmetry properties it directly follows that reversing the direction of the magnetic field is equivalent to the down-turn bend and the previous orientation of the field.[82,83] This situation is shown in Fig. 1(b). Similar nonequivalence of the up- and down-turn bends occurs for the curved waveguide with the transversely asymmetric embedded quantum dot in zero field.[62] Due to the fixed direction of the particle motion in the uniform magnetic field, now we need to choose the polar axis coinciding with the other junction between the curved and straight sections and the azimuthal angle ϕ growing again in the counterclockwise direction, as shown by the curved arrow in Fig. 1(b). Accordingly, Eqs. (27) will also be changed:

$$(x_1=0, y_1) \Leftrightarrow \left(y_1+\rho_0+\tfrac{1}{2}, \phi=0\right), \tag{30a}$$

$$(x=0, y) \Leftrightarrow \left(y+\rho_0+\tfrac{1}{2}, \phi=\phi_0\right), \tag{30b}$$

$$\left.\frac{\partial}{\partial x_1}\right|_{x_1=0} \Leftrightarrow -\frac{1}{y_1+\rho_0+\frac{1}{2}} \left.\frac{\partial}{\partial \phi}\right|_{\phi=0}, \tag{30c}$$

$$\left.\frac{\partial}{\partial x}\right|_{x=0} \Leftrightarrow -\frac{1}{y+\rho_0+\frac{1}{2}} \left.\frac{\partial}{\partial \phi}\right|_{\phi=\phi_0}. \tag{30d}$$

In all other aspects, the procedure of deriving the scattering **S** and reflection **R** matrices remains the same as described above.

When one considers the bound state lying below the fundamental propagation threshold of the straight arm, it is necessary to put all coefficients C_n in Eq. (9) equal to zero, $C_n \equiv 0$. The procedure of matching is completely similar to the one used for the scattering case, and leads then to the infinite linear algebraic system. Requirement of the vanishing of its determinant defines energies of the bound levels. Corresponding equations for both turns are provided in the Appendix. An infinite set of eigenvectors corresponding to the eigenenergies defines coefficients D_n, F_n, and Q_n. In other words, one can fully construct bound-state wave functions in the magnetic field.

III. RESULTS AND DISCUSSION

In this section we provide results of the calculations of the bound levels and scattering states according to the theory developed in Sec. II. For finding the conductance G we confine our consideration to the fundamental propagation mode only, $E_1^{TH} \leqslant E \leqslant E_2^{TH}$, thus eliminating a possibility of obscuring the most characteristic features of discussed phenomena by the wave interference from different subbands. From the multichannel reciprocity theorem[122] and mirror-plane symmetry of the system,[83] it follows that in this case there is no difference between up- and down-turn bends. Moreover, as our calculations show, bound-state energies do not depend on the direction of the magnetic field either. This is consistent with previous studies of similar systems.[91] Thus, in the following, we will talk about the magnitude of the magnetic field B only, without reference to the up- or down-turn configuration.

A. Bound state

We start from the discussion of the bound state. Figure 4 shows its energy as a function of the magnetic field for several values of ρ_0 and ϕ_0. For comparison, lowest solutions of Eqs. (18) and (22) are also shown. The bound-state energy monotonically increases with B. At high fields it approaches from below the fundamental propagation threshold of the straight arm which, in turn, lies in this regime very close to the lowest Landau level B/π^2. For smaller radii and larger angles this asymptotic transformation takes place at stronger fields. This is due to the fact that sharper bends present a larger perturbation to the electron motion and, accordingly,

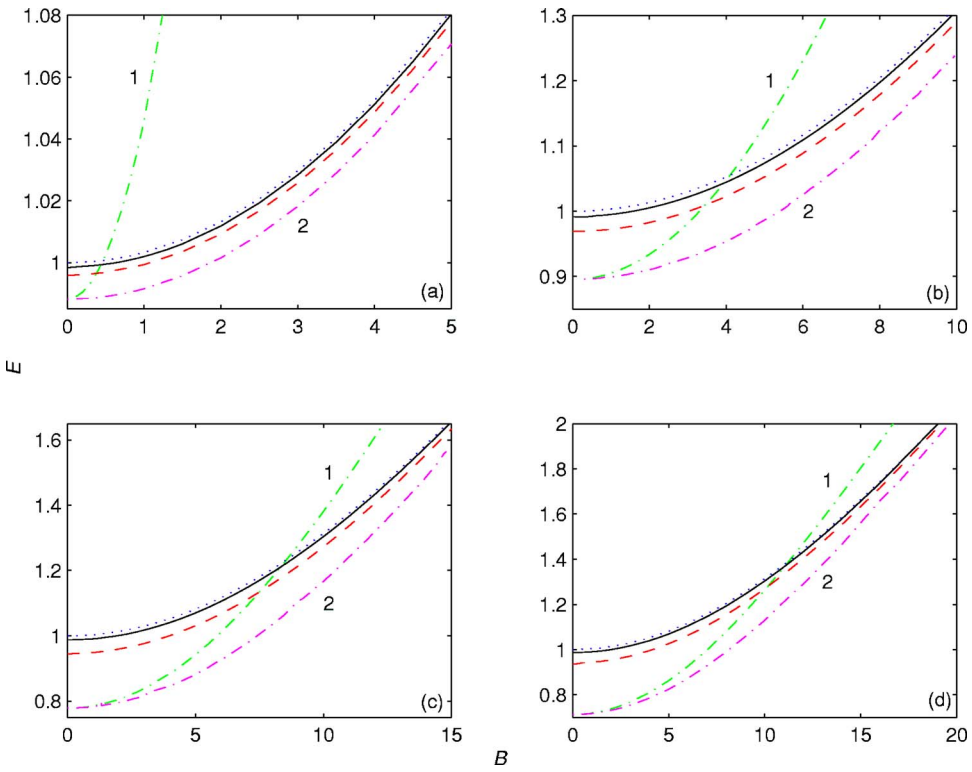

FIG. 4. (Color online) Bound state energies as a function of applied magnetic field B for bend radius (a) $\rho_0=1$, (b) $\rho_0=0.1$, (c) $\rho_0=0.01$, and (d) $\rho_0=0.001$ and angle $\phi_0=90°$ (solid line) and $\phi_0=180°$ (dashed line). Fundamental propagation threshold for the straight arm is shown by the dotted curve. Dash-dotted line 1 is the lowest solution of Eq. (18) while the dash-dotted curve 2 depicts the least solution of Eq. (22). Note different axes scales for each of the figures.

higher B are needed to come to purely magnetic quantization. Recently, it was proved theoretically that differentiable bounded magnetic fields with compact support can wipe out localized states of the bent waveguide.[94] In other words, a nonuniform field vanishing at infinity creates such repulsive effective potential that it is able to neutralize the attractiveness of the bend "seen" by the electron. However, this is not the case for the uniform fields where bound states always exist. For small magnetic fields its properties are determined by the electrostatic potential of the bent waveguide, and at high B one has mainly magnetic quantization. Such a transition from electric to magnetic quantization is a general feature of all quantum systems in uniform magnetic fields.[11,13,14] In particular, it was shown in Ref. 11 that a true bound state of a four-terminal junction at high B also approaches nodeless Landau level. Thus, one can deduce that the bound state of any bent channel exists at arbitrary homogeneous magnetic fields. However, general proof of this statement for an arbitrary bent waveguide, with arms asymptotically straight at infinity, is missing in any literature known to us.

Dash-dotted lines in Fig. 4 vividly show the difference between the solutions of Eqs. (18) and (22). As we discussed in the previous section, for $B=0$ they are identical. However, first one of them grows faster with magnetic field with its steepness determined by the bend radius, and at some value of B passes the fundamental threshold of the straight waveguide. Whenever it crosses bound-state energy, it means that for the higher fields the localized level is described by the negative angular wave vectors only. This is a subtle peculiarity of the magnetic field case compared to the situation with $B=0$ when both ν are equal in magnitude and have opposite signs. In its turn, solutions of Eq. (22) for nonzero fields play the role of the propagation thresholds in the continuously curved wire since they are always lower than cutoff energies for the straight arms. For the field-free case it is a necessary condition of the existence of bound states.[35,63] As we can see, the same requirement holds true if we associate the solutions of Eq. (22) with the propagation thresholds of the curved wire. Then, as Fig. 4 shows, bound-state energies lie in the range between cutoff energies of the straight and bent parts, as in the case for the field-free situation. This range shrinks with magnetic field growing. As a result, angular wave vectors of localized levels are always real but, contrary to the zero-field case, both of them may be negative, which reflects the fact that the clockwise and counterclockwise directions of the electron motion in uniform magnetic field are not equivalent.

Bound-state wave functions of the right angle bend with $\rho_0=0.001$ are shown in Fig. 5 for different values of the magnetic field B. Increasing the magnetic field suppresses the transverse distribution of the wave function in the straight arms and simultaneously squeezes it closer to the bent region. For the very strong fields, the wave function is localized mainly in the bend, where it tries to build up its shape corresponding to the lowest Landau level. For all fields the wave function remains symmetric with respect to the line $\phi=\phi_0/2$.

B. Transport in the fundamental mode

1. Conductance

Next, we turn to the scattering configuration. For the field-free case an introduction of the bend leads to the situation when immediately after the lower threshold, the conductance from zero rapidly grows with energy and very soon approaches values close to unity.[35,39,46] Evolution of the con-

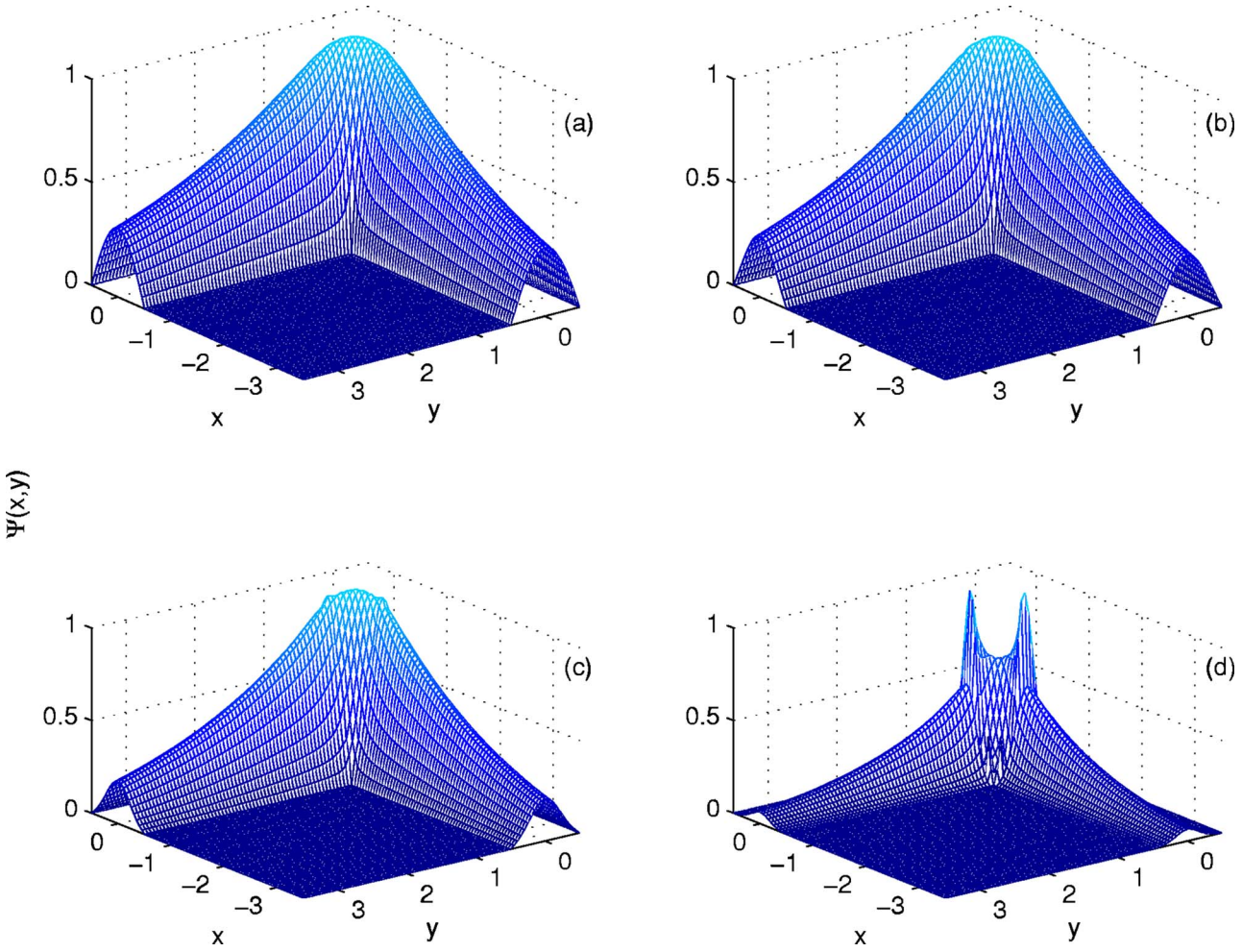

FIG. 5. (Color online) Wave function $\Psi(x,y)$ (normalized to its maximum) of the bound state for $\rho_0=0.001$ and the right angle for (a) $B=0$, (b) $B=10$, (c) $B=20$, and (d) $B=35$.

ductance near the subband's lower threshold in magnetic fields was discussed in Ref. 84 and will not be addressed here. For the field-free case, another remarkable feature of the conductance-energy dependence of the curved waveguide is a steep antiresonance slightly below the upper boundary of each propagating mode of the straight wire. Interference of the discrete level split off by the bend from the higher lying subband, with the continuum states of the lower mode causes the conductance to drop abruptly, and for the fundamental propagation subband, to vanish at some energy E_{min}, which is determined by the parameters of the bend.[35,39] Thus, at this point we have a complete interference blockade of the electron transport. The resonance is characterized by the energy E_{min} where zero minimum of the conductance is achieved, and by its half width Γ, which defines the lifetime τ of the quasibound state,

$$\tau = \frac{1}{\Gamma}. \tag{31}$$

Without the field, at fixed ρ_0 the value of Γ is an oscillating function of ϕ_0, and at some bend angles it turns to zero, which corresponds to the formation of the true bound state in the continuum which, according to Eq. (31), has an infinite lifetime.[39]

Applying the field modifies drastically transport properties of the wire. Figure 6 shows conductance Fermi energy dependence at several magnetic fields for the bend with $\rho_0=0.001$ and $\phi_0=180°$. It is seen that the magnetic field leads to the right shift of the energy E_{min} at which the minimum is achieved. As shown in Fig. 6, conductance in the minimum G_{min}, generally, ceases to be zero for nonvanishing magnetic fields. For example, for $\rho_0=0.001$ and $\phi_0=180°$, initially it monotonically grows with B. At $B=3.66$ value G_{min} reaches its maximum equal to unity, $G_{min}=1$, which means that the resonance is completely dissolved. Further growth of the intensity B causes G_{min} to decrease, and at $B=5.34$ the minimum of the conductance reaches zero again after which it resumes its growth. Thus, we see that, in addition to the parameters E_{min} and Γ, which completely describe the corresponding resonance for $B=0$, in the magnetic field one needs to introduce the resonance minimum value G_{min}. Moreover, a definition of the half width Γ itself should be generalized to cover the case of nonzero G_{min}; namely, now it is the difference between the energies at which the value of the conductance $G=(1+G_{min})/2$ is achieved. For the magnetic fields

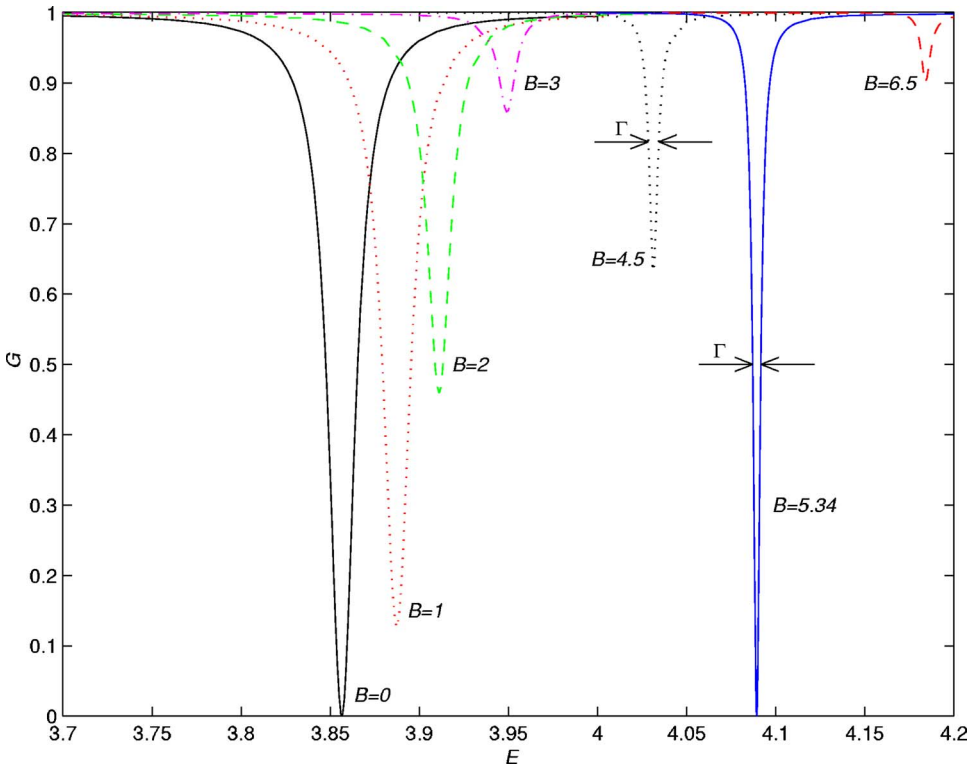

FIG. 6. (Color online) Conductance G as a function of the Fermi energy E for the bend with $\rho_0=0.001$ and $\phi_0=180°$ for several values of the magnetic field B. Numbers near the curves denote corresponding intensity B. Arrows show half widths Γ for $B=4.5$ and $B=5.34$.

$B=4.5$ and $B=5.34$ corresponding half widths Γ are shown by the arrows in Fig. 6.

Figures 7 and 8 show, respectively, G_{min} and Γ as functions of the magnetic field for several ρ_0 and ϕ_0. E_{min} monotonically increases with B and at high fields approaches the first excited Landau level $3B/\pi^2$. Since this behavior is very similar to the one discussed in Fig. 4, it is not shown here. It is seen that for the large enough bend radii, say, $\rho_0=0.5$ in Figs. 7 and 8, the minimum of the conductance grows quite rapidly with B for the bend angle $\phi_0=180°$, and at moderate fields of $B=2.5$ it reaches a value of unity at which it stays with magnetic intensity growing. This means that the quasibound level formed as a result of the bend is completely dissolved. As Figs. 7 and 8 show, for the smaller angles this

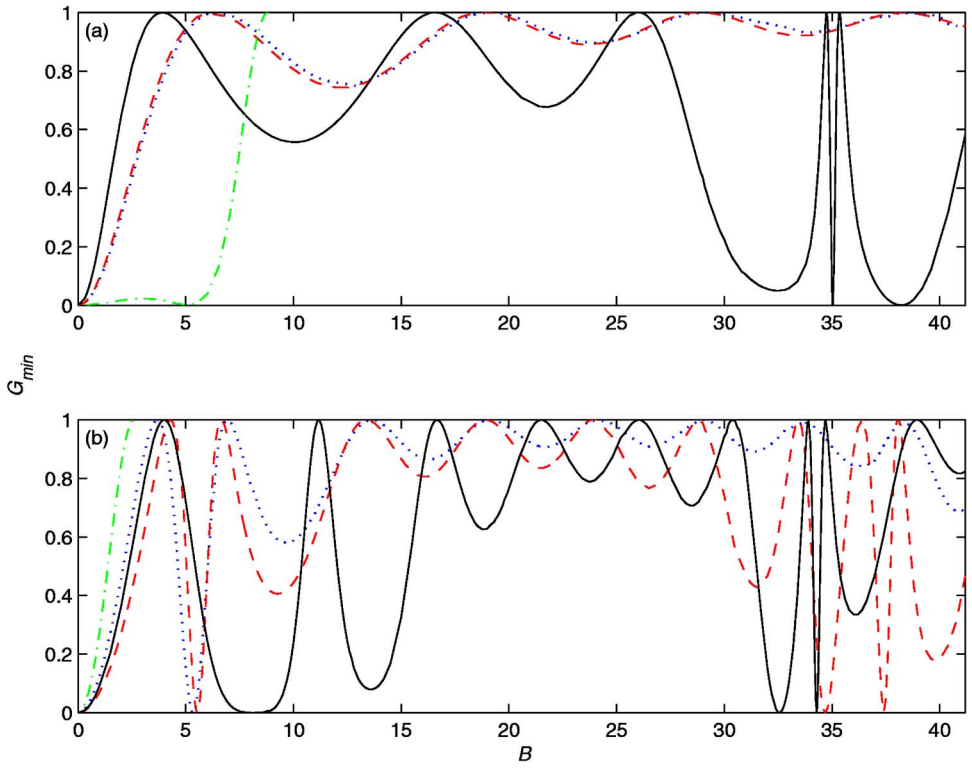

FIG. 7. (Color online) Conductance G_{min} corresponding to the minimum on G-E curve as a function of the field B for the bend angle (a) $\phi_0=90°$ and (b) $\phi_0=180°$ and several values of the bend radius ρ_0 where the dash-dotted line corresponds to $\rho_0=0.5$, the solid line is for $\rho_0=0.1$, the dashed line is for $\rho_0=0.01$, and the dotted line is for $\rho_0=0.001$.

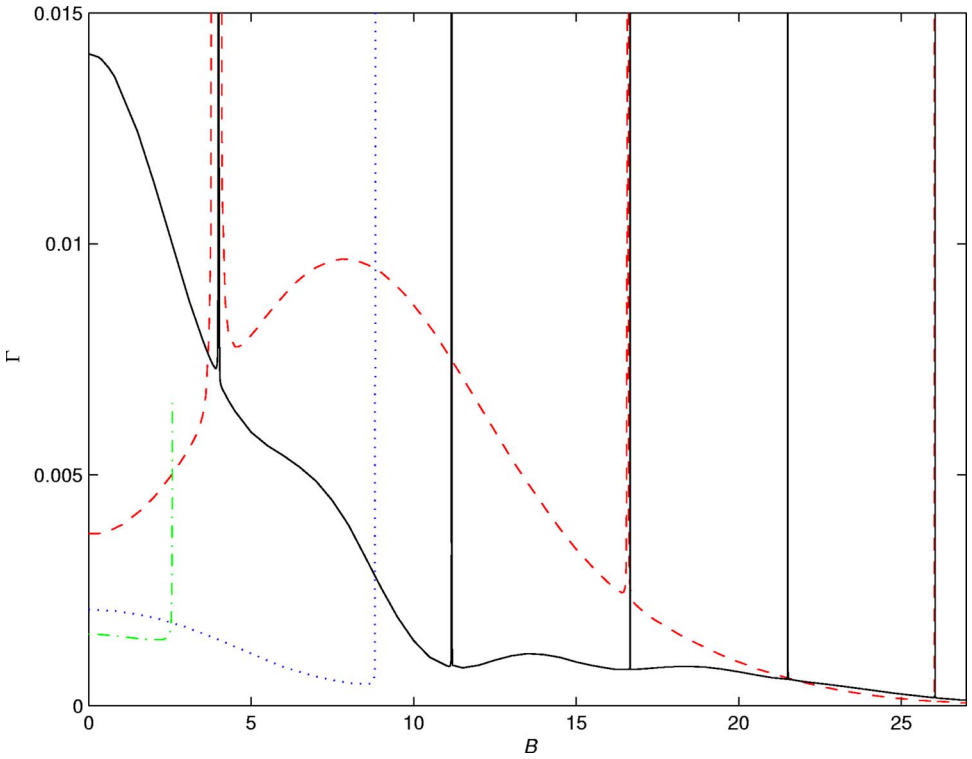

FIG. 8. (Color online) Half width Γ as a function of magnetic field B for $\rho_0=0.1$ and $\phi_0=180°$ (solid line), $\rho_0=0.1$ and $\phi_0=90°$ (dashed line), $\rho_0=0.5$ and $\phi_0=180°$ (dash-dotted line), and $\rho_0=0.5$ and $\phi_0=90°$ (dotted line).

happens at larger magnetic fields; for example, for the right angle G_{min} reaches unity at about $B=8.8$. Dissolution of the quasibound level is manifested in Fig. 8 where half widths Γ have rapid peaks at the magnetic fields corresponding to G_{min} approaching unity. Growing half widths mean, according to Eq. (31), a drastic reduction of the lifetime of the corresponding quasibound level. The Γ curve for $\rho_0=0.5$ and $\phi_0=180°$ is terminated at $B=2.571$ since for the higher fields the conductance on the G-E dependence after passing the very shallow minimum G_{min} cannot reach again with energy growing the value of $(1+G_{min})/2$ staying almost flat instead. In other words, we cannot talk anymore about quasibound levels since these levels have been completely wiped out by the magnetic field. As Fig. 8 shows, the magnitude of B where this happens, and corresponding to it, the critical value of Γ, depend on the bend parameters ρ_0 and ϕ_0. We note that for the large radii the magnetic length $l_B=B^{-1/2}$ at which this complete dissolution takes place, is almost proportional to the bend angle ϕ_0. For example, at $\rho_0=0.5$ this critical length is equal to 0.34 for $\phi_0=90°$, and to 0.63 for $\phi_0=180°$. We remark that the minimum conductance for $\phi_0=45°$ (not shown here) reaches its maximum of unity at approximately the same field when G_{min} for the right angle saturates. However, for the smaller angle, after passing this extremum, the conductance G_{min} decreases with a further increase of B, reaches minimum, grows again, and merges with the unity at the magnetic field with the length l_B being about one-half of the above-mentioned value for $\phi_0=90°$. In other words, quasibound states of the bent channel with smaller angles are more resilient with respect to the magnetic field. This unexpected result seems to contradict the fact that larger bend angles bind electron stronger. In particular, it is known that for the field-free case energies, E_{min} monotonically decrease with ϕ_0 (see Fig. 3 in Ref. 39). Also, as we mentioned above, bound states in the magnetic field for the smaller angles are stronger perturbed by the field; in particular, they approach Landau levels at smaller B. To explain this seeming discrepancy, we mention that for the large enough radius a straightening transformation is applicable; namely, one can substitute a curved section by the straight one-dimensional quantum well of depth $V_{\rho_0}=1/[2\pi(\rho_0+\frac{1}{2})]^2$ and width $L=(\rho_0+1/2)\phi_0$, where angle ϕ_0 is measured in radians.[36] Thus, at $B=0$ for the smaller angles the wave function of the bound level below the fundamental cutoff energy is less localized in the curved section and it penetrates stronger into the straight arms. Accordingly, applied magnetic field influences such states more strongly, since for small B its vector potential becomes noticeable at large distances only. On the contrary, quasibound states in the first propagating mode are formed as a result of the interference mainly in the curved section. As a result, smaller magnetic fields with larger l_B influence this interference for the waveguides with larger ϕ_0 only when the well width is also larger. Quasibound states for small bend angles remain intact since for them small magnetic fields perturb motion mainly in the straight elbows. In other terms, we can say that a total magnetic flux Φ through the bend

$$\Phi = B\left(\rho_0 + \tfrac{1}{2}\right)\phi_0 \tag{32}$$

is proportional to the bend angle ϕ_0 and, accordingly, quasibound states are perturbed more strongly by the field for larger ϕ_0. Deviations from this linear dependence for smaller angles are due to the fact that for higher B electron behavior deviates more strongly from the purely one-dimensional picture valid at zero fields. In particular, for large magnetic fields the current flow is not symmetric with respect to the

middle plane of the channel. For small ρ_0 we will discuss this phenomenon below.

The situation becomes even more complicated for the small radii. As Fig. 7 shows, for $\rho_0 \leqslant 0.1$ minimum conductance oscillates as a function of the magnetic field when $\rho_0 \leqslant l_B$. Minimal value of G_{min}, in each minimum, increases with B while each maximum, $G_{min}=1$ is accompanied by the divergence of the half width, as was discussed above and is shown in Fig. 8. The number of these maxima is larger for the larger bend angle. For the very small bend radii in this range of the fields further decrease of ρ_0 does not alter significantly G_{min} dependence; for example, for $B<30$ there is no considerable difference between the curves for $\rho_0=0.01$ and 0.001 in Fig. 7. Qualitatively, this is in accordance with the straightening transformation described above where for the very small ρ_0 its variation almost has no effect on the quantum well characteristics. We note that in this range of the fields the half width Γ, even far away from its divergences, is a nonmonotonic function of the intensity B. Its particular behavior is determined by the bend parameters ϕ_0 and ρ_0 with a general tendency of decreasing Γ for quite strong fields. It is also worth noting that widths of the resonances on the Γ-B dependence diminish with the magnetic field growing.

For the still higher magnetic fields when $l_B \lesssim \rho_0$, rapid oscillations of G_{min} between zero and unity develop as a function of B. For example, for $\rho_0=0.1$ and $\phi_0=180°$ minimum of the conductance reaches zero at $B=32.6$ ($l_B=0.175$) and $B=34.3$ ($l_B=0.171$). Maxima of G_{min}, as before, are equal to unity. After passing these zero minima, conductance G_{min} has several other minima on the B axis where, however, it is larger than zero and increases with B. With further growth of the field, G_{min} merges with unity with the corresponding divergence of Γ as described above for $\rho_0=0.5$. This means that the quasibound level is completely dissolved. Other essential features of this transformation include the fact that zero minima for the smaller bend radius ρ_0 are achieved at higher fields; for example, for $\rho_0=0.01$ and $\phi_0=180°$, they are located at $B=34.7$ ($l_B=0.170$) and $B=37.4$ ($l_B=0.164$), and for $\rho_0=0.001$ they lie beyond the range of $B \leqslant 40$. Also, similar to the larger bend radius case discussed above, these minima for the smaller bend angle occur at the higher fields, as comparison of panels (a) and (b) shows in Fig. 7.

2. Current density

Conductance is determined by the currents flowing in the waveguide. Thus, in order to explain conductance phenomena described above, we found it instructive to study currents flowing in the waveguide. Current density in the magnetic field is given as[121]

$$\mathbf{j} = -\mathrm{Im}[\Psi^*(\mathbf{r})\,\boldsymbol{\nabla}\,\Psi(\mathbf{r})] - \mathbf{A}\Psi^*(\mathbf{r})\Psi(\mathbf{r}). \qquad (33)$$

It is known that for the straight channel with impurity in the perpendicular homogeneous magnetic field two-dimensional current density $\mathbf{j}$ forms vortices at the energies near the resonances on G-E curves.[17,123,124] In turn, for the field-free bent waveguide the vortices develop near E_{min} also.[37,45,50,55,62,63,79] Contrary to the vortices in the superfluid and superconductor[125,126] or the semiconductor in the regime of fractional quantum Hall effect[2,3] which are formed as a result of interparticle interaction, the vortices we consider here are a product of the geometry-related wave interference only, and their characteristic feature is the abrupt change of the direction of their rotation when energy passes through E_{min}.[37,55,62,63]

For the bent waveguide in the magnetic field $\mathbf{B}$ we start our discussion from the case of small and moderate magnetic fields. Figure 9 shows current density evolution with the Fermi energy changing for the down-turn curved waveguide with $\rho_0=0.001$ and $\phi_0=180°$ at magnetic field $B=1$ (see the corresponding curve in Fig. 6). Far away from the resonance, the current flow is perfectly laminar both in the straight parts as well as in the curved section. When the energy comes closer to E_{min}, vortices start to develop in the bend. One of the initial phases of the formation of the vortices is shown in Fig. 9(a) where the transverse component of $\mathbf{j}$, which was zero for the smaller energies, is clearly observable inside and near the bend. Far away in the straight arms the current still has a longitudinal component only. A small increase in the energy leads to the formation of the vortices in the bend [Fig. 9(b)]. The current magnitude in the vortex is a few orders of magnitude larger than for the flow far away from the bend. Contrary to the field-free case (see, e.g., Fig. 10 in Ref. 63), vortices develop in the bend only. In the straight arms instead of the circular vortices we see surface currents[24,117–119] flowing along the wire boundaries as well as junctions with the bend. Instead of the vortices, these interacting with each other currents form, depending on the energy, more or less developed *antivortices*. Another difference is the unequal strength of the vortices. For example, vortices near the junctions are resolved much better than their counterpart in the middle of the bend while for $B=0$ all of them have the same magnitude.[63] A further slight increase of the energy leads to the clockwise motion of the vortices as a whole. This is clearly seen in Fig. 9(c), where the center of the lower vortex reached the junction, and only its right half is observable with the left part being dissolved in the straight arm where a new antivortex is formed. After passing E_{min} this vortex is completely dissolved, and near the upper junction the new vortex starts to develop [Fig. 9(d)]. As the energy grows, the upper vortex is completely formed with its magnitude equal to the strength of the new lower vortex, as shown in Fig. 9(e). However, both of them are smaller than the strength of the central vortex. In other words, compared to the situation with $E<E_{min}$ [Fig. 9(b)], central and junction vortices have exchanged their magnitudes. Another difference of parts (b) and (e) in Fig. 9 is the opposite angular direction of currents for each vortex. Thus, similar to the field-free case,[37,55,63] vortices have different rotation directions on the opposite sides of E_{min}; however, transformation from one direction to the other is different for $B=0$ and $B\neq 0$. As we move further from the resonance, the vortices dissolve with junction vortices disappearing faster than the central counterpart [Fig. 9(f)]. Comparative analysis of parts (f) and (a) provides the same results as the previous discussion for panels (e) and (b).

So, we have found that for small and moderate $\mathbf{B}$ current density evolution acquires new features absent at zero field.

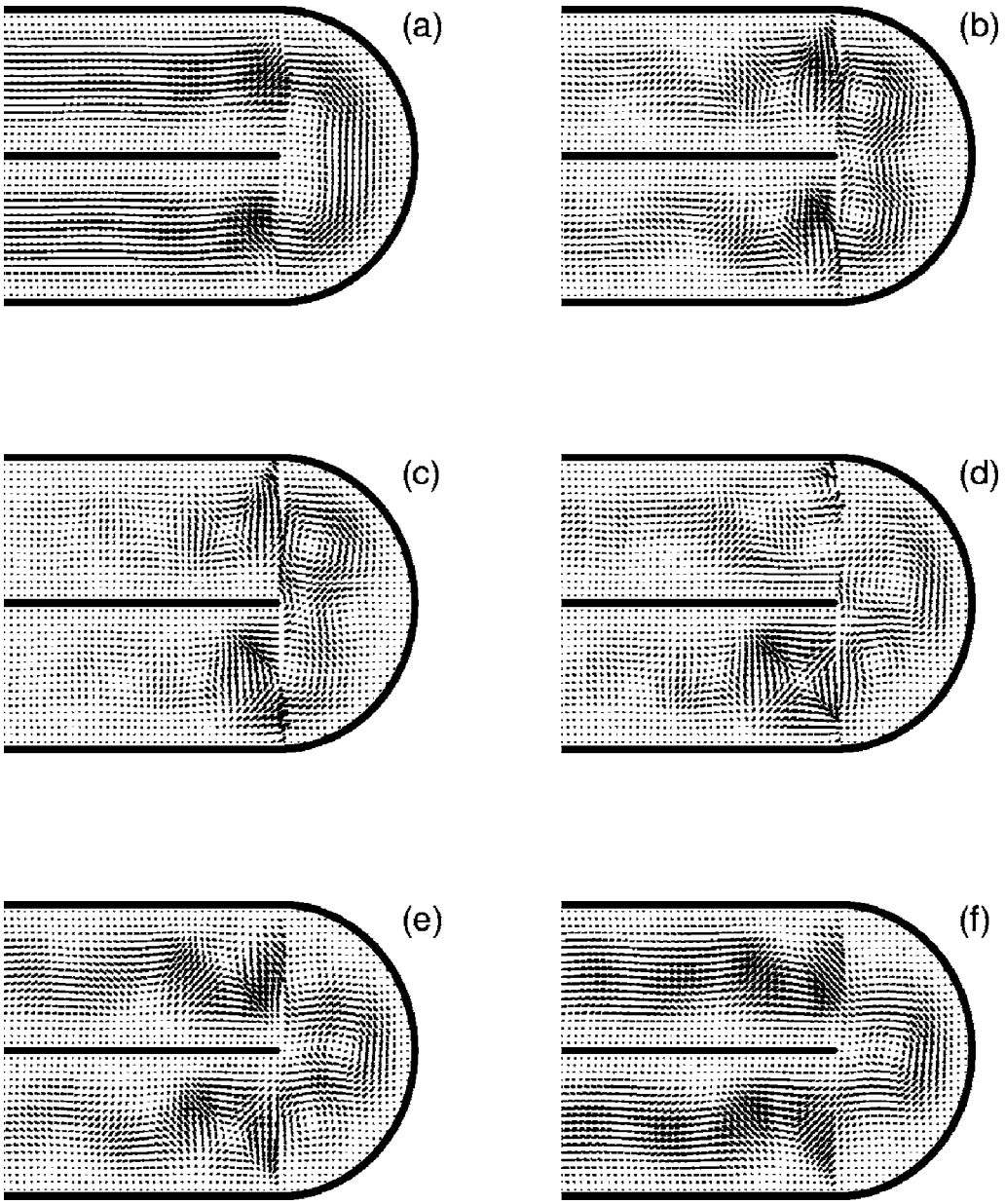

FIG. 9. Spatial distribution of the current densities **j** at magnetic field $B=1$ for $\rho_0=0.001$, $\phi_0=180°$ and several values of the energy E: (a) $E=3.8$ (conductance $G=0.9884$), (b) $E=3.87$ ($G=0.7993$), (c) $E=3.885$ ($G=0.1803$), (d) $E=3.892$ ($G=0.2983$), (e) $E=3.905$ ($G=0.8122$), (f) $E=3.94$ ($G=0.9753$). Since the bend radius is very small, the distance between two parallel inner walls is not seen in the figure. Larger arrows denote higher currents. For each of the figures the currents are normalized with respect to their largest value.

The picture is changed even more with magnetic intensity growing. Namely, currents in the straight arms far away from the resonance are pushed stronger and stronger to the outer waveguide boundaries. This is known as the edge-state regime on which the theory of the integer quantum Hall effect is based.[2,3,5] In its turn, azimuthal currents in the bend for the larger B concentrate near the inner surface. This situation is shown in the panel (a) of Fig. 10 which shows current densities for $\rho_0=0.01$ and $\phi_0=180°$ and magnetic field $B=34.7$ corresponding to the zero minimum of G_{min} in Fig. 7(b). In the straight (bent) part, currents near the outer (inner) walls are a few orders of magnitude higher than that close to the inner (outer) boundaries. It means that there is a transverse charge flow along the junctions between straight arms and the curved section. Since this current is conspicuous near the very neighborhood of the junctions only, it is not resolved on the grid of Fig. 10. The half width in the considered case is very small, $\Gamma=0.000\,001$; accordingly, very slight changes in the energy have a large impact on the conductivity G and currents flowing in the waveguide. For example, a transition from the energy of the panel (a) to the one of the part (b) is accompanied by the transformation of the laminar flow in the bend into the single vortex rotating in the clockwise direction. In both cases, however, the conductance is equal to unity. Contrary to the case of small fields, no multiple vortices are formed in the bend. In the straight arms, the current basically still retains a laminar flow and is concentrated near the outer plates. As one comes closer to the minimum, the

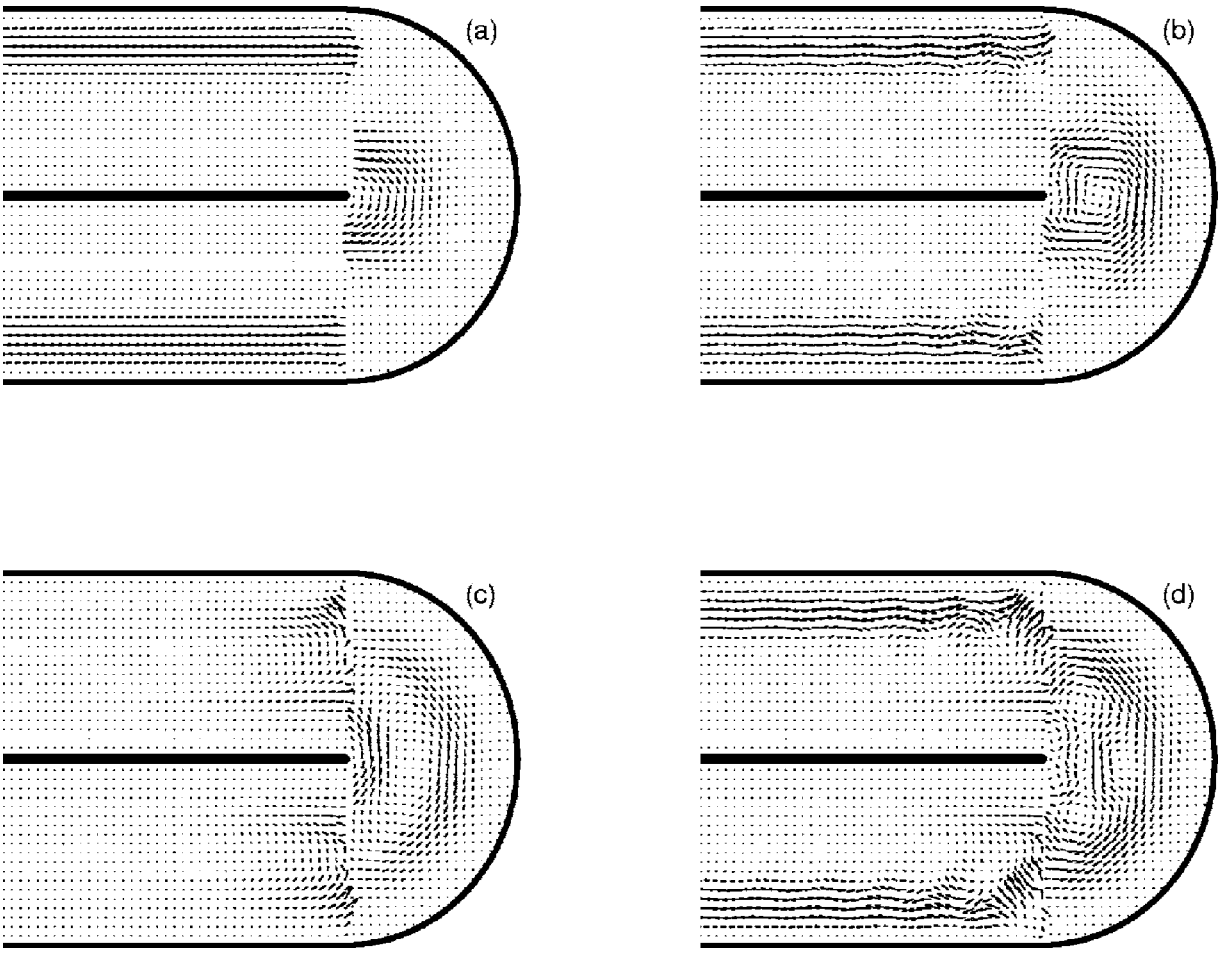

FIG. 10. Spatial distribution of the current densities **j** at magnetic field $B=34.7$ for $\rho_0=0.01$, $\phi_0=180°$ and energies: (a) $E=10.575$, (b) $E=10.5805$, (c) $E=10.5810474$, and (d) $E=10.5815$. For panel (c) conductance G is zero while for all other figures it is practically indistinguishable from unity.

vortex loses its circular shape acquiring instead the form of the bent part with the largest currents flowing in the counterclockwise direction near the inner edge and in clockwise direction in the middle of the curved section. Figure 10(c) shows such current distributions when the exact minimum is achieved, $G_{min}=0$. These currents are a few orders of magnitude larger than the flow far away from the bend. They also are much larger than the currents shown in the other panels of Fig. 10. The interference between the counterclockwise and clockwise flows determines the total transmission of the waveguide. In this range of the fields tiny changes in B vary current distribution near the inner curved surface which, in turn, drastically changes the conductance, as seen in Fig. 7. The direction of the vortex rotation does not change after passing the minimum, as was the case for $B=0$ (Refs. 37, 55, and 63) or for small fields discussed above. When one moves to the right from the minimum E_{min}, the bent-shaped vortex is sprayed into the irregular structure, typical form of which is shown in Fig. 10(d). One sees here a number of vortices with their strength, however, being six orders of magnitude smaller than the one from the panel (c). In the straight arms the current restores the laminar flow in the edge-state regime.

Thus, comparing Figs. 9 and 10, one sees that increasing magnetic field suppresses the formation of the vortices near the resonance: five vortices at $B=0$ change to the three ones at $B=1$, and are substituted by one rotation only at $B\sim 35$. At even higher fields, currents are pushed stronger and stronger to the outer (inner) surface in the straight (bent) part of the waveguide. On the one hand, this explains why zero minima of G_{min} for the larger bend radius take place at smaller B when magnetic length l_B is also larger. On the other hand, the fields sufficiently far to the right of these minima forbid formation of any vortices at all as they press the electron stronger and stronger to the convex surface; as a result, one has perfect laminar flows both in the straight and bent parts for all energy values. Absence of the vortices in this case means that the conductance remains equal to unity for all energies; in other words, the quasibound state is completely dissolved by the increasing magnetic field; traversing the electron for such large intensities B does not "see" anymore bend as an obstacle for its motion. The only consequence of the bend in this case is transverse currents flowing along junctions between straight and bent parts of the quantum wire, and azimuthal currents near the inner curved surface.

IV. CONCLUDING REMARKS

We have considered theoretically properties of the curved quantum wire in homogeneous perpendicular magnetic fields. It was shown that bound states below the fundamental propagation threshold of such a system always exist, approaching for high fields, the lowest Landau level. Depending on the magnetic intensity and bend parameters, they can be described by the wave function with the same sign of the angular wave vectors that reflects the nonequivalence of the clockwise and counterclockwise directions in the magnetic field. For the scattering case, dips in the conductance appearing as a result of the bend dissolve for high magnetic fields, which means that the quasibound state in the propagation mode has been eliminated. For smaller bend angles and radii these quasibound levels survive stronger fields. The magnetic field also strongly affects the current vortices near the conductance minimum; for example, at small **B** zero-field vortices in the straight arms transform into the magnetic antivortices.

As we already mentioned, for the field-free case at some critical bend parameters the half width Γ turns to zero[39] which, according to Eq. (31), leads to the existence of the bound state in the continuum with an infinite lifetime. For quantum systems, the existence of such very special solutions of the Schrödinger equation was predicted theoretically soon after the formulation of the wave mechanics.[127] They received a lot of theoretical attention,[17,30,39,62,63,128–134] and were detected experimentally in semiconductor superlattices.[135,136] At $B=0$, for the curved waveguide the bound states in the continuum have $\Gamma=0$ and $G_{\min}=1$. The applied small magnetic field **B** leads to the growth of the half width and decrease of the minimum conductance. In other words, the magnetic field turns the true bound state in the continuum into the quasibound state with finite lifetime. A similar situation takes place for the straight channel with attractive impurity.[17] In both cases, the magnetic field mixes transverse and longitudinal motions in the wire, thus coupling true localized state with the continuum, and, accordingly, turning it into the quasibound level with finite lifetime. Thus, for the true bound state in the continuum at zero field the difference with the situation considered before in the text is the fact that a curve in Fig. 7 starts from $G_{\min}=1$ at $B=0$ instead of $G_{\min}=0$ for the quasibound state. In the same way, in Fig. 8, the half width Γ grows from zero. In all other aspects, this level behavior in the magnetic fields is the same as discussed above.

For the bend radius $\rho_0 \leqslant 0.1$ rapid oscillations of $G_{\min}$ take place at magnetic fields $B > 30$. Of course, in this regime applicability of the effective mass approximation[101] should be additionally justified. Moreover, for such high fields effects of electron-electron correlations become crucial in defining system properties. However, results presented here should serve as a basis for more advanced treatment where Coulomb scattering is explicitly taken into account. In particular, it would be of both theoretical as well as experimental importance to investigate interaction between geometry-induced vortices studied here, and rotations emerging in the fractional quantum Hall effect as a result of electron-electron scattering.[2,3]

Finally, we point out that recently a curved channel with different boundary conditions was considered theoretically for the field-free case.[61,63,137,138] Physically, this situation corresponds, for example, to the superconductor sandwiched between dielectric and nonsuperconducting metals,[125,126] to the electromagnetic wave propagation between the Earth and ionosphere[139,140] or to the continental shelf waves.[138] It was shown that if the Dirichlet boundary condition is applied to the inner (outer) surface, and the Neumann one—to the other strip, then waveguide properties mimic the ones with the Dirichlet (Neumann) requirements on both confining walls. In wake of the research carried out in the present paper, it is of interest to calculate the curved waveguide with different boundary conditions in uniform magnetic fields. These results will be published elsewhere.

ACKNOWLEDGMENT

L.M. acknowledges the hospitality of the Abdus Salam International Center for Theoretical Physics (Trieste, Italy) where part of this project was done.

APPENDIX

Scattering $\mathbf{S}(E)$ and reflection $\mathbf{R}(E)$ matrices of the bent waveguide in uniform magnetic field are given as

$$\mathbf{S} = \pm \mathbf{P}_1 \mathbf{\Phi} (\mathbf{I} \mp \mathbf{P}_2^T \mathbf{P}_2)^{-1} \mathbf{P}_1^T, \tag{A1a}$$

$$\mathbf{R} = \pm \mathbf{P}_2 (\mathbf{I} \mp \mathbf{P}_2^T \mathbf{P}_2)^{-1} \mathbf{P}_1^T, \tag{A1b}$$

where $\mathbf{I}$ is the infinite identity matrix, superscript T denotes a transposed matrix, and infinite matrices $\mathbf{P}_i$, $i=1,2$, and $\mathbf{\Phi}$ have the following elements:

$$(\mathbf{P}_1)_{nn'} = \int_{-1/2}^{1/2} \left(p_n \pm \frac{\nu_{n'}}{\mp y + \rho_0 + \frac{1}{2}} + \tfrac{1}{2} B\left(-3y \pm \rho_0 \pm \tfrac{1}{2}\right) \right) \times \chi_{p_n}(y) R_{\nu_{n'}}\left(\mp y + \rho_0 + \tfrac{1}{2}\right) dy \tag{A2a}$$

$$(\mathbf{P}_2)_{nn'} = \int_{-1/2}^{1/2} \left(-p_n \pm \frac{\nu_{n'}}{\mp y + \rho_0 + \frac{1}{2}} + \tfrac{1}{2} B\left(-3y \pm \rho_0 \pm \tfrac{1}{2}\right) \right) \chi_{-p_n}(y) R_{\nu_{n'}}\left(\mp y + \rho_0 + \tfrac{1}{2}\right) dy \tag{A2b}$$

$$\Phi_{nn'} = \exp(\pm i \nu_n \phi_0) \delta_{nn'}. \tag{A2c}$$

In the above equations, upper (lower) signs correspond to up(down)-turn bend. Bound-state energies are determined

from the following two equations for up- and down-turn bends, respectively:

$$\det\|\mathbf{I}-\mathbf{P}_2^T\mathbf{P}_2+(\mathbf{I}-\mathbf{P}_1^T\mathbf{P}_1)\mathbf{\Phi}\|=0, \tag{A3a}$$

$$\det\|\mathbf{I}+\mathbf{P}_1^T\mathbf{P}_1+(\mathbf{I}+\mathbf{P}_2^T\mathbf{P}_2)\mathbf{\Phi}^{-1}\|=0. \tag{A3b}$$

Similar to the field-free case,[39] in the literature[141–143] there are no explicit expressions for the integrals in the matrices $\mathbf{P}_i$, $i=1,2$. Therefore, we performed their direct numerical quadrature.

*Present address: Department of Physics, Jackson State University, Jackson, MS 39217, USA; E-mail: oleg.olendski@jsums.edu

[1] K. v. Klitzing, G. Dorda, and M. Pepper, Phys. Rev. Lett. **45**, 494 (1980).

[2] *The Quantum Hall Effect*, edited by P. R. Prange and S. M. Girvin (Springer-Verlag, New York, 1990).

[3] T. Chakraborty and P. Pietiläinen, *The Quantum Hall Effects: Integral and Fractional* (Springer-Verlag, Berlin, 1995).

[4] A. H. MacDonald, in *Mesoscopic Quantum Physics*, edited by E. Akkermans, G. Montambaux, J.-L. Pichard, and J. Zinn-Justin, Proceedings of the 1994 Les Houches Summer School, Session LXI (Elsevier, Amsterdam, 1995), p. 659.

[5] K. I. Wysokiński, Eur. J. Phys. **21**, 535 (2000).

[6] T. Koma, Rev. Math. Phys. **16**, 1115 (2004).

[7] J. K. Jain and S. A. Kivelson, Phys. Rev. B **37**, 4276 (1988).

[8] P. H. M. van Loosdrecht, C. W. J. Beenakker, H. van Houten, J. G. Williamson, B. J. van Wees, J. E. Mooij, C. T. Foxon, and J. J. Harris, Phys. Rev. B **38**, 10162 (1988).

[9] F. M. Peeters, Phys. Rev. Lett. **61**, 589 (1988).

[10] G. Kirczenow, Phys. Rev. Lett. **62**, 1920 (1989); **62**, 2993 (1989); Phys. Rev. B **42**, 5357 (1990).

[11] D. G. Ravenhall, H. W. Wyld, and R. L. Schult, Phys. Rev. Lett. **62**, 1780 (1989); R. L. Schult, H. W. Wyld, and D. G. Ravenhall, Phys. Rev. B **41**, 12760 (1990).

[12] H. U. Baranger, D. P. DiVincenzo, R. A. Jalabert, and A. D. Stone, Phys. Rev. B **44**, 10637 (1991).

[13] A. H. MacDonald and P. Středa, Phys. Rev. B **29**, 1616 (1984).

[14] W. Zawadzki, Semicond. Sci. Technol. **2**, 550 (1987); O. Z. Olendskiĭ, Fiz. Tverd. Tela (S.-Peterburg) **34**, 3087 (1992) [Sov. Phys. Solid State **34**, 1653 (1992)].

[15] C. S. Kim and O. Olendski, Appl. Phys. Lett. **69**, 2575 (1996); Semicond. Sci. Technol. **12**, 788 (1997).

[16] U. Fano, Phys. Rev. **124**, 1866 (1961).

[17] J. U. Nöckel, Phys. Rev. B **46**, 15348 (1992).

[18] R. Akis, P. Vasilopoulos, and P. Debray, Phys. Rev. B **56**, 9594 (1997).

[19] P. Duclos, P. Exner, and B. Meller, Rep. Math. Phys. **47**, 253 (2001).

[20] V. Vargiamidis and H. M. Polatoglou, Phys. Rev. B **67**, 245303 (2003).

[21] V. Gudmundsson, Y.-Y. Lin, C.-S. Tang, V. Moldoveanu, J. H. Bardarson, and A. Manolescu, Phys. Rev. B **71**, 235302 (2005).

[22] J. U. Nöckel and A. D. Stone, Phys. Rev. B **51**, 17219 (1995).

[23] M. L. Roukes, A. Scherer, S. J. Allen, Jr., H. G. Craighead, R. M. Ruthen, E. D. Beebe, and J. P. Harbison, Phys. Rev. Lett. **59**, 3011 (1987).

[24] M. Büttiker, Phys. Rev. B **38**, 9375 (1988).

[25] W. Rostafinski, *Monograph on Propagation of Sound Waves in Curved Ducts* (NASA Scientific and Technical Information Division, Washigton, D.C., 1991).

[26] J. A. Cochran and R. G. Pecina, Radio Sci. **1**, 679 (1966).

[27] C. P. Bates, Bell Syst. Tech. J. **49**, 2259 (1969).

[28] L. Lewin, D. C. Chang, and E. F. Kuester, *Electromagnetic Waves and Curved Structures* (Peter Peregrinus, Stevenage, UK, 1977).

[29] B. Z. Katsenelenbaum, L. Mercader del Río, M. Pereyaslavets, M. Sorolla Ayza, and M. Thumm, *Theory of Nonuniform Waveguides* (IEE, London, UK, 1998).

[30] R. L. Schult, D. G. Ravenhall, and H. W. Wyld, Phys. Rev. B **39**, 5476 (1989).

[31] P. Exner and P. Šeba, J. Math. Phys. **30**, 2574 (1989); P. Exner, Phys. Lett. A **141**, 213 (1989); P. Exner, P. Šeba, and P. Štoviček, Czech. J. Phys., B **39**, 1181 (1989); Phys. Lett. A **150**, 179 (1990); M. S. Ashbough and P. Exner, *ibid.* **150**, 183 (1990); P. Exner, J. Math. Phys. **34**, 23 (1993); J. Phys. A **28**, 5323 (1995).

[32] Y. Avishai, D. Bessis, B. G. Giraud, and G. Mantica, Phys. Rev. B **44**, 8028 (1991).

[33] J. Goldstone and R. L. Jaffe, Phys. Rev. B **45**, 14100 (1992).

[34] J. P. Carini, J. T. Londergan, K. Mullen, and D. P. Murdock, Phys. Rev. B **46**, 15538 (1992); **48**, 4503 (1993); J. P. Carini, J. T. Londergan, D. P. Murdock, D. Trinkle, and C. S. Yung, *ibid.* **55**, 9842 (1997).

[35] F. Sols and M. Macucci, Phys. Rev. B **41**, 11887 (1990).

[36] D. W. L. Sprung, H. Wu, and J. Martorell, J. Appl. Phys. **71**, 515 (1992); H. Wu, D. W. L. Sprung, and J. Martorell, Phys. Rev. B **45**, 11960 (1992).

[37] K.-F. Berggren and Z.-L. Ji, Phys. Rev. B **47**, 6390 (1993).

[38] K. Lin and R. L. Jaffe, Phys. Rev. B **54**, 5750 (1996).

[39] O. Olendski and L. Mikhailovska, Phys. Rev. B **66**, 035331 (2002).

[40] P. Duclos and P. Exner, Rev. Math. Phys. **7**, 73 (1995).

[41] J. T. Londergan, J. P. Carini, and D. P. Murdock, *Binding and Scattering in Two-dimensional Systems: Applications to Quantum Wires, Waveguides, and Photonic Crystals* (Springer-Verlag, Berlin, 1999).

[42] F. Lenz, J. T. Londergan, E. J. Moniz, R. Rosenfelder, M. Stingl, and K. Yazaki, Ann. Phys. (N.Y.) **170**, 65 (1986).

[43] H. Eyring, J. E. Walter, and G. E. Kimball, *Quantum Chemistry* (Wiley, New York, 1944), Chap. 16.

[44] H. M. Hulburt and J. O. Hirschfelder, J. Chem. Phys. **11**, 276 (1943); K. T. Tang, B. Kleinman, and M. Karplus, *ibid.* **50**, 1119 (1969); P. D. Robinson, *ibid.* **52**, 3175 (1970); D. R. Dion, M. B. Milleur, and J. O. Hirschfelder, *ibid.* **52**, 3179 (1970).

[45] J. O. Hirschfelder and K. T. Tang, J. Chem. Phys. **64**, 760 (1976).

[46] C. S. Lent, Appl. Phys. Lett. **56**, 2554 (1990).

[47] H. U. Baranger, Phys. Rev. B **42**, 11479 (1990).

[48] A. Weisshaar, J. Lary, S. M. Goodnick, and V. K. Tripathi, Appl. Phys. Lett. **55**, 2114 (1989); J. C. Wu, M. N. Wybourne, W.

Yindeepol, A. Weisshaar, and S. M. Goodnick, *ibid.* **59**, 102 (1991); Q. W. Shi, J. Zhou, and M. W. Wu, *ibid.* **85**, 2547 (2004).

[49] S. Takagi and T. Tanzawa, Prog. Theor. Phys. **87**, 561 (1992).

[50] H. Wu and D. W. L. Sprung, Phys. Lett. A **183**, 413 (1993).

[51] Y. B. Gaididei and O. O. Vakhnenko, J. Phys.: Condens. Matter **6**, 3229 (1994); O. O. Vakhnenko, Phys. Rev. B **52**, 17386 (1995); Phys. Lett. A **211**, 46 (1996); **231**, 419 (1997).

[52] J. P. Carini, J. T. Londergan, and D. P. Murdock, Phys. Rev. B **55**, 9852 (1997).

[53] M. Razavy, Phys. Rev. A **55**, 4102 (1997); Int. J. Mod. Phys. B **12**, 1907 (1998).

[54] C.-K. Wang, Physica B **229**, 240 (1997).

[55] E. Šimánek, Phys. Rev. B **59**, 10152 (1999).

[56] A. I. Vedernikov and A. V. Chaplik, Zh. Eksp. Teor. Fiz. **117**, 449 (2000) [JETP **90**, 397 (2000)]; L. I. Magarill, D. A. Romanov, and A. V. Chaplik, Usp. Fiz. Nauk **170**, 325 (2000) [Phys. Usp. **43**, 283 (2000)]; L. I. Magarill and M. V. Éntin, Zh. Eksp. Teor. Fiz. **123**, 867 (2003) [JETP **96**, 766 (2003)]; A. V. Chaplik and R. H. Blick, New J. Phys. **6**, 33 (2004); A. V. Chaplik, Pis'ma Zh. Eksp. Teor. Fiz. **80**, 140 (2004) [JETP Lett. **80**, 130 (2004)]; L. I. Magarill, A. V. Chaplik, and M. V. Éntin, Usp. Fiz. Nauk **175**, 995 (2005) [Phys. Usp. **48**, 953 (2005)].

[57] E. Granot, Phys. Rev. B **60**, 14172 (1999); **65**, 233101 (2002).

[58] P. Duclos, P. Exner, and D. Krejčiřík, Ukr. Fiz. Zh. **45**, 595 (2000) [Ukr. Phys. J. **45**, 595 (2000)]; Commun. Math. Phys. **223**, 13 (2001); P. Exner and T. Ichinose, J. Phys. A **34**, 1439 (2001); P. Exner and D. Krejčiřík, *ibid.* **34**, 5969 (2001); D. Krejčiřík and R. T. de Aldecoa, *ibid.* **37**, 5449 (2004); P. Exner and V. A. Zagrebnov, *ibid.* **38**, L463 (2005).

[59] I. Y. Popov, Phys. Lett. A **269**, 148 (2000).

[60] A. Namiranian, M. R. H. Khajehpour, Y. A. Kolesnichenko, and S. N. Shevchenko, Physica E (Amsterdam) **10**, 549 (2001).

[61] J. Dittrich and J. Kříž, J. Phys. A **35**, L269 (2002).

[62] O. Olendski and L. Mikhailovska, Phys. Rev. B **67**, 035310 (2003).

[63] O. Olendski and L. Mikhailovska, Phys. Rev. E **67**, 056625 (2003).

[64] M. Encinosa and L. Mott, Phys. Rev. A **68**, 014102 (2003); L. Mott, M. Encinosa, and B. Etemadi, Physica E (Amsterdam) **25**, 521 (2004).

[65] D. Levin, J. Phys. A **37**, L9 (2004).

[66] P. Ouyang, V. Mohta, and R. L. Jaffe, Ann. Phys. (N.Y.) **275**, 297 (1999); P. C. Schuster and R. L. Jaffe, *ibid.* **307**, 132 (2003).

[67] R. Y. Chiao and Y.-S. Wu, Phys. Rev. Lett. **57**, 933 (1986); A. Tomita and R. Y. Chiao, *ibid.* **57**, 937 (1986).

[68] A. Weisshaar, S. M. Goodnick, and V. K. Tripathi, IEEE Trans. Microwave Theory Tech. **40**, 2200 (1992); B. Gimeno and M. Guglielmi, *ibid.* **44**, 1679 (1996); P. Cornet, R. Dusséaux, and J. Chandezon, *ibid.* **47**, 965 (1999); A. A. San Blas, B. Gimeno, V. E. Boria, H. Esteban, S. Cogollos, and A. Coves, *ibid.* **51**, 397 (2003).

[69] E. N. Bulgakov and A. F. Sadreev, Zh. Tekh. Fiz. **71** (10), 77 (2001) [Tech. Phys. **46**, 1281 (2001)]; Phys. Rev. B **66**, 075331 (2002).

[70] M. Spivack, J. Ogilvy, and C. Sillence, Waves Random Media **12**, 47 (2002).

[71] P. Ylä-Oijala, J. Sarvas, and M. Taskinen, Electromagnetics **23**, 27 (2003); I. V. Petrusenko, *ibid.* **24**, 237 (2004).

[72] J.-T. Kim and J.-G. Ih, Appl. Acoust. **56**, 297 (1999); S. Félix and V. Pagneux, J. Acoust. Soc. Am. **110**, 1329 (2001); **116**, 1921 (2004); Wave Motion **36**, 157 (2002); **41**, 339 (2005).

[73] S.-X. Qu and M. R. Geller, Phys. Rev. B **70**, 085414 (2004).

[74] D. Müller, D. Z. Anderson, R. J. Grow, P. D. D. Schwindt, and E. A. Cornell, Phys. Rev. Lett. **83**, 5194 (1999); N. Blanchard and A. Zozulya, Opt. Commun. **190**, 231 (2001); P. Leboeuf and N. Pavloff, Phys. Rev. A **64**, 033602 (2001).

[75] S. F. Mingaleev and Y. S. Kivshar, Opt. Lett. **27**, 231 (2002); S. F. Mingaleev and K. Busch, *ibid.* **28**, 619 (2003).

[76] Y. Kokubun, A. Miura, and S. Inokuchi, Jpn. J. Appl. Phys. **43**, 8080 (2004).

[77] A. Talneau, M. Mulot, S. Anand, S. Olivier, M. Agio, M. Kafesaki, and C. M. Soukoulis, Photonics Nanostruct. Fundam. Appl. **2**, 1 (2004).

[78] M. W. J. Bromley and B. D. Esry, Phys. Rev. A **68**, 043609 (2003); **69**, 053620 (2004).

[79] M. W. J. Bromley and B. D. Esry, Phys. Rev. A **70**, 013605 (2004).

[80] C. Gorria, Y. B. Gaididei, M. P. Soerensen, P. L. Christiansen, and J. G. Caputo, Phys. Rev. B **69**, 134506 (2004); Y. B. Gaididei, P. L. Christiansen, P. G. Kevrekidis, H. Büttner, and A. R. Bishop, New J. Phys. **7**, 52 (2005).

[81] O. Post, J. Phys. A **38**, 4917 (2005).

[82] K. Vacek, H. Kasai, and A. Okiji, J. Phys. Soc. Jpn. **61**, 27 (1992).

[83] K. Vacek, A. Okiji, and H. Kasai, Phys. Rev. B **47**, 3695 (1993).

[84] J. J. Palacios and C. Tejedor, Phys. Rev. B **48**, 5386 (1993).

[85] Y. Aharonov and D. Bohm, Phys. Rev. **115**, 485 (1959). Literature on the Aharonov-Bohm effect is too huge to mention it all. Excellent reviews describing the efforts in the nonrelativistic field, are given in S. Olariu and I. I. Popescu, Rev. Mod. Phys. **57**, 339 (1985); V. D. Skarzhinskiy, Tr. Fiz. Inst. Akad. Nauk SSSR **167**, 139 (1986) [Proc. Lebedev Phys. Inst., Acad. Sci. USSR **167**, 176 (1987)]; V. G. Bagrov, D. M. Gitman, and V. D. Skarzhinskiy, *ibid.* **176**, 151 (1986) [*ibid.* **176**, 201 (1988)]; M. Peshkin and A. Tonomura, *The Aharonov-Bohm Effect* (Springer, Berlin, 1989); G. N. Afanas'ev, Fiz. Elem. Chastits At. Yadra **21**, 172 (1990) [Sov. J. Part. Nucl. **21**, 74 (1990)]; J. Hamilton, *Aharonov-Bohm and Other Cyclic Phenomena* (Springer, Berlin, 1997). Some recent publications try to bring a fresh new insight on this phenomenon: C. Magni and F. Valz-Gris, J. Math. Phys. **36**, 177 (1995); A. G. Chirkov and A. N. Ageev, Zh. Tekh. Fiz. **71** (2), 16 (2001) [Tech. Phys. **46**, 147 (2001)]; Fiz. Tverd. Tela (S.-Peterburg) **44**, 3 (2002) [Phys. Solid State **44**, 1 (2002)]; Y. Aharonov and T. Kaufherr, Phys. Rev. Lett. **92**, 070404 (2004). Criticism of commonly accepted interpretation was raised recently by T. H. Boyer, Found. Phys. **30**, 893 (2000); **30**, 907 (2000); **32**, 1 (2002); **32**, 41 (2002).

[86] G. Dunne and R. L. Jaffe, Ann. Phys. (N.Y.) **223**, 180 (1993).

[87] M. Melgaard, Few-Body Syst. **35**, 77 (2004).

[88] P. Exner, Phys. Lett. A **178**, 236 (1993).

[89] E. N. Bulgakov and A. F. Sadreev, Pis'ma Zh. Eksp. Teor. Fiz. **66**, 403 (1997) [JETP Lett. **66**, 431 (1997)]; Zh. Eksp. Teor. Fiz. **114**, 1954 (1998) [JETP **87**, 1058 (1998)].

[90] V. A. Geĭler and I. Y. Popov, Pis'ma Zh. Tekh. Fiz. **27**(11), 7 (2001) [Tech. Phys. Lett. **27**, 444 (2001)].

[91] Y.-K. Lin, Y.-N. Chen, and D.-S. Chuu, J. Appl. Phys. **91**, 3054 (2002).

[92] B.-Y. Gu, Y.-K. Lin, and D.-S. Chuu, J. Appl. Phys. **86**, 1013 (1999); K.-Q. Chen, B.-Y. Gu, Y.-K. Lin, and D.-S. Chuu, Int. J.

Mod. Phys. B **13**, 903 (1999).
[93] O. O. Vakhnenko, Phys. Lett. A **249**, 349 (1998).
[94] T. Ekholm and H. Kovařík, Commun. Partial Differ. Equ. **30**, 539 (2005).
[95] C. J. B. Ford, S. Washburn, M. Büttiker, C. M. Knoedler, and J. M. Hong, Phys. Rev. Lett. **62**, 2724 (1989).
[96] K. Amemiya and K. Kawamura, J. Phys. Soc. Jpn. **63**, 3087 (1994).
[97] R. Rinaldi, R. Cingolani, M. Lepore, M. Ferrara, I. M. Catalano, F. Rossi, L. Rota, E. Molinari, P. Lugli, U. Marti, D. Martin, F. Morier-Gemoud, P. Ruterana, and F. K. Reinhart, Phys. Rev. Lett. **73**, 2899 (1994).
[98] T. Someya, H. Akiyama, and H. Sakaki, Phys. Rev. Lett. **74**, 3664 (1995).
[99] A. Tsukernik, A. Palevski, V. J. Goldman, S. Luryi, E. Kapon, and A. Rudra, Phys. Rev. B **63**, 153315 (2001).
[100] Y. K. Kato, R. C. Myers, A. C. Gossard, and D. D. Awschalom, Appl. Phys. Lett. **87**, 022503 (2005).
[101] J. M. Luttinger and W. Kohn, Phys. Rev. **97**, 869 (1955).
[102] J. C. P. Miller, *Tables of Weber Parabolic Cylinder Functions* (Her Majesty Stationery Office, London, UK, 1955); I. E. Kireeva and K. A. Karpov, *Tables of Weber Functions* (Pergamon Press, Oxford, UK, 1961); H. Bateman and A. Erdélyi, *Higher Transcendental Functions* (McGraw-Hill, New York, 1953), Vol. 2.
[103] *Handbook of Mathematical Functions*, edited by M. Abramowitz and I. A. Stegun (Dover, New York, 1964).
[104] K. Amemiya, J. Phys. Soc. Jpn. **68**, 567 (1999); **68**, 1464 (1999); **72**, 135 (2003).
[105] L. Landau, Z. Phys. **64**, 629 (1930).
[106] K. Vacek, A. Okiji, and H. Kasai, Phys. Rev. B **48**, 11412 (1993).
[107] H. Bateman and A. Erdélyi, *Higher Transcendental Functions* (McGraw-Hill, New York, 1953), Vol. 1.
[108] L. Page, Phys. Rev. **36**, 444 (1930).
[109] F. Geerinckx, F. M. Peeters, and J. T. Devreese, J. Appl. Phys. **68**, 3435 (1990).
[110] C. S. Lent, Phys. Rev. B **43**, 4179 (1991).
[111] N. C. Constantinou, M. Masale, and D. R. Tilley, J. Phys.: Condens. Matter **4**, 4499 (1992); **4**, L293 (1992); M. Masale, N. C. Constantinou, and D. R. Tilley, Phys. Rev. B **46**, 15432 (1992); Supercond. Sci. Technol. **6**, 287 (1993); M. Masale and N. C. Constantinou, Phys. Rev. B **48**, 11128 (1993); M. Masale, Physica B **291**, 256 (2000); Physica C **377**, 75 (2002); Phys. Scr. **67**, 260 (2003); Supercond. Sci. Technol. **18**, 661 (2003).
[112] Y. Avishai, Y. Hatsugai, and M. Kohmoto, Phys. Rev. B **47**, 9501 (1993); Y. Avishai and M. Kohmoto, Phys. Rev. Lett. **71**, 279 (1993).
[113] E.-X. Ping and V. Dalal, J. Appl. Phys. **76**, 2547 (1994).
[114] L. Solimany and B. Kramer, Solid State Commun. **96**, 471 (1995); G. Ihm, N. Kim, H.-S. Sim, K.-H. Ahn, K. J. Chang, and S. J. Lee, Physica B **249**, 291 (1998); H.-S. Sim, K.-H. Ahn, K. J. Chang, G. Ihm, N. Kim, and S. J. Lee, Phys. Rev. Lett. **80**, 1501 (1998); N. Kim, G. Ihm, H.-S. Sim, and K. J. Chang, Phys. Rev. B **60**, 8767 (1999); R. Rosas, R. Riera, and J. L. Marín, J. Phys.: Condens. Matter **12**, 6851 (2000); B. Kocsis, G. Palla, and J. Cserti, Phys. Rev. B **71**, 075331 (2005).
[115] C. S. Kim and O. Olendski, Phys. Rev. B **53**, 12917 (1996); O. Olendski and C. S. Kim, J. Phys.: Condens. Matter **8**, 2197 (1996); J. Korean Phys. Soc. **31**, 461 (1997).
[116] J. Reijniers, F. M. Peeters, and A. Matulis, Phys. Rev. B **59**, 2817 (1999).
[117] B. I. Halperin, Phys. Rev. B **25**, 2185 (1982).
[118] M. Robnik, J. Phys. A **19**, 3619 (1986).
[119] T.-L. Ho, Phys. Rev. B **50**, 4524 (1994).
[120] R. Landauer, IBM J. Res. Dev. **1**, 223 (1957); **32**, 306 (1988); Philos. Mag. **21**, 863 (1970).
[121] L. D. Landau and E. M. Lifshitz, *Quantum Mechanics (Non-Relativistic Theory)* (Pergamon, New York, 1977).
[122] M. Büttiker, Phys. Rev. Lett. **57**, 1761 (1986); IBM J. Res. Dev. **32**, 317 (1988).
[123] V. Marigliano Ramaglia, F. Ventriglia, and G. P. Zucchelli, Phys. Rev. B **48**, 2445 (1993).
[124] A. Nakamura and S. Nonoyama, Phys. Rev. B **56**, 9649 (1997).
[125] D. R. Tilley and J. Tilley, *Superfluidity and Superconductivity* (Van Nostrand, New York, 1974).
[126] L. D. Landau and E. M. Lifshitz, *Statistical Physics* (Pergamon, New York, 1980), Pt. 2.
[127] J. von Neumann and E. Wigner, Z. Phys. **30**, 465 (1929).
[128] F. H. Stillinger and D. R. Herrick, Phys. Rev. A **11**, 446 (1975); D. R. Herrick and F. H. Stillinger, J. Chem. Phys. **62**, 4360 (1975); D. R. Herrick, Physica B **85**, 44 (1977); F. H. Stillinger, *ibid.* **85**, 270 (1977); H. Friedrich and D. Wintgen, Phys. Rev. A **31**, 3964 (1985); **32**, 3231 (1985).
[129] A. Lami and N. K. Rahman, Phys. Rev. A **33**, 782 (1986); **34**, 3908 (1986); **41**, 2901 (1990); C. A. Glosson and C. D. Cantrell, *ibid.* **41**, 2898 (1990).
[130] I. Y. Popov and S. L. Popova, Phys. Lett. A **222**, 286 (1996); V. A. Geyler and I. Y. Popov, Rep. Math. Phys. **39**, 275 (1997); I. Y. Popov, *ibid.* **40**, 521 (1997); **43**, 427 (1999).
[131] C. S. Kim and A. M. Satanin, Zh. Eksp. Teor. Fiz. **115**, 211 (1999) [JETP **88**, 118 (1999)]; Teor. Mat. Fiz. **120**, 116 (1999) [Theor. Math. Phys. **120**, 910 (1999)]; Physica E (Amsterdam) **4**, 211 (1999); C. S. Kim, A. M. Satanin, Y. S. Joe, and R. M. Cosby, Phys. Rev. B **60**, 10962 (1999); Zh. Eksp. Teor. Fiz. **116**, 263 (1999) [JETP **89**, 144 (1999)].
[132] E. N. Bulgakov, P. Exner, K. N. Pichugin, and A. F. Sadreev, Phys. Rev. B **66**, 155109 (2002).
[133] D. W. L. Sprung, P. Jagiello, J. D. Sigetich, and J. Martorell, Phys. Rev. B **67**, 085318 (2003).
[134] D. V. Evans, C. M. Linton, and F. Ursell, Q. J. Mech. Appl. Math. **46**, 253 (1993); D. V. Evans, M. Levitin, and D. Vassiliev, J. Fluid Mech. **261**, 21 (1994).
[135] C. Sirtori, F. Capasso, J. Faist, D. L. Sivco, S.-N. G. Chu, and A. Y. Cho, Appl. Phys. Lett. **61**, 898 (1992); F. Capasso, C. Sirtori, J. Faist, D. L. Sivco, S.-N. G. Chu, and A. Y. Cho, Nature (London) **358**, 565 (1992).
[136] B. Sung, H. C. Chui, E. L. Martinet, and J. S. Harris, Jr., Appl. Phys. Lett. **68**, 2720 (1996).
[137] D. Krejčiřík and J. Kříž, Publ. Res. Inst. Math. Sci. **41**, 757 (2005).
[138] E. R. Johnson, M. Levitin, and L. Parnovski, math.SP/0409575, SIAM J. Math. Anal. (to be published).
[139] K. Davies, *Ionospheric Radio* (Peter Peregrinus, London, UK, 1991).
[140] S. F. Mahmoud, *Electromagnetic Waveguides: Theory and Applications* (Peter Peregrinus, London, UK, 1991).

[141] I. S. Gradshteyn and I. M. Ryzhik, *Table of Integrals, Series, and Products* (Academic, New York, 2000).

[142] A. P. Prudnikov, Yu. A. Brychkov, and O. I. Marichev, *Integrals and Series* (Gordon and Breach Science Publishers, New York, 1986), Vol. 2.

[143] A. P. Prudnikov, Yu. A. Brychkov, and O. I. Marichev, *Integrals and Series* (Gordon and Breach Science Publishers, New York, 1990), Vol. 3.